# A Unified and Scalable Framework for the Comprehensive Evaluation of Hydrological Model Behavior and Structural Diagnostics

Carlos Erazo Ramirez[1*], Yusuf Sermet[1], Ali Jannesari[2], Chaoqun Lu[3], Ibrahim Demir[1,4]

[1] ByWater Institute, Tulane University

[2] Computer Science, Iowa State University

[3] Soil and Environmental Sciences, University of Wisconsin-Madison

[4] River-Coastal Science and Engineering, Tulane University

[*] Corresponding Author, cerazoramirez@tulane.edu

## Abstract

Robust evaluation of hydrological models requires assessing not only predictive accuracy, but also uncertainty behavior and structural realism. This study introduces the Hydrological Model Evaluation System (HyMES), a unified framework that organizes deterministic, probabilistic, and structural diagnostics, including dynamic hysteresis analysis, into a coherent, station-level evaluation workflow. HyMES is implemented as a fully browser-based application, enabling interactive, reproducible analysis without local installations. The framework is demonstrated through a comparative evaluation of retrospective streamflow simulations from the National Water Model (NWM v2.1 and v3.0) across stations in the Mississippi River region for 2010–2023. Results show that modest deterministic improvements in newer model versions often arise from compensatory error structures and do not consistently translate to improved uncertainty robustness or structural behavior. Structural and hysteresis diagnostics reveal persistent deficiencies in flow variability, seasonal organization, and catchment memory that are masked by aggregate metrics. HyMES provides a scalable, transparent platform for diagnosing hydrological model behavior beyond single-metric performance assessment.

## Keywords

Model diagnostics; Ensemble Evaluation; Hydroinformatics; Web-based Tools

## Software Availability

| | |
|---|---|
| Name | Hydrologic Model Evaluation System - HyMES |
| Developers | Carlos Erazo Ramirez, Khoa D. Le |
| Contact Information | https://hydroinformatics.tulane.edu |
| Software required | Web Browser |
| Programming language | JavaScript, WASM, R |
| Platform Access | https://hydroinformatics.tulane.edu/lab/hymes/ |
| Data | Case study data is available within the platform |

This manuscript is an EarthArXiv preprint and has been submitted for possible publication in a peer reviewed journal. Please note that this has not been peer-reviewed before and is currently undergoing peer review for the first time. Subsequent versions of this manuscript may have slightly different content.

## 1. Introduction

Hydrological models are commonly evaluated using a range of statistical and diagnostic approaches intended to assess predictive skill, physical consistency, and uncertainty. Over several decades, three complementary strands of evaluation practice have emerged within the hydrological sciences: deterministic performance metrics, which summarize agreement between simulated and observed flows; probabilistic methods, which quantify uncertainty and sensitivity under parametric, structural, or forcing variability; and hydrological signature diagnostics, which evaluate whether simulated time series reproduce physically meaningful flow behaviors (Yilmaz et al., 2008; Addor et al., 2020; McMillan et al., 2016; Ewing et al., 2024). Collectively, these approaches form the basis of contemporary hydrological model evaluation. Despite the wide adoption of these methods, however, they are often applied independently or selectively in practice. Evaluations are frequently shaped by study-specific objectives, analyst expertise, or tool availability, resulting in fragmented and difficult-to-reproduce analyses (Thébault et al., 2024; Gupta et al., 2014; Newman et al., 2015). This separation limits the ability to interpret model behavior holistically and complicates comparative evaluation across models, stations, or modeling generations.

Robust evaluation of hydrological models requires methodologies capable of assessing not only predictive accuracy, but also uncertainty representation and structural realism (Moriasi et al., 2007; Moriasi et al., 2015; Lane et al., 2019) utilizing streamlined benchmark datasets and model configurations (Ebert-Uphoff et al., 2017; Kizilkaya et al., 2025; Sit et al., 2021). As hydrological models have increased in complexity, incorporating higher spatial resolution, more explicit process representations, and ensemble-based forecasting capabilities, the need for evaluation frameworks that move beyond single-score assessment has become increasingly evident (Ewing et al., 2022). Contemporary hydrological evaluation practice has therefore coalesced around three complementary paradigms: deterministic performance metrics, probabilistic uncertainty methods, and structural or signature-based diagnostics. Each paradigm offers insight into a distinct dimension of model behavior, yet each also exhibits fundamental limitations when applied in isolation. Understanding these paradigms, their strengths, and their inherent tensions is essential for motivating unified, multi-layer evaluation frameworks.

### 1.1. Deterministic Performance Metrics

Deterministic performance metrics have historically formed the cornerstone of hydrological model evaluation due to their simplicity, interpretability, and low computational cost. Metrics such as the Nash–Sutcliffe Efficiency (NSE) and Root Mean Square Error (RMSE) summarize predictive agreement between simulated and observed discharge using aggregate error formulations rooted in classical least-squares theory (Nash & Sutcliffe, 1970; Schaefli & Gupta, 2007; Legates & McCabe, 1999; Demir et al., 2022). Among these metrics, the Kling–Gupta Efficiency (KGE; Gupta et al., 2009; Kling et al., 2012; Tang et al., 2021) represents a significant methodological advance by decomposing performance into physically interpretable components: correlation (temporal dynamics), variability ratio (dispersion and extremes), and bias ratio (long-term water balance). This decomposition diagnostic helps identifying whether deficiencies arise from timing errors, misrepresentation of flow variability, or volumetric inconsistencies.

However, deterministic metrics remain fundamentally reductionist. They collapse complex, temporally structured model behavior into scalar quantities, overshadowing regime-dependent performance and masking compensatory errors (Clark et al., 2021; Sivelle et al., 2023; Ritter & Muñoz-Carpena, 2013; Boyle et al., 2000). A model may achieve high deterministic efficiency by reproducing peak flows accurately while simultaneously misrepresenting baseflow persistence or seasonal recession dynamics. Moreover, deterministic scores offer no explicit representation of uncertainty and are inherently sensitive to sampling variability, benchmark selection, and flow regime dominance (Knoben et al., 2019; Krause et al., 2005; Melsen et al., 2025; McCuen et al., 2006).

### 1.2. Probabilistic and Uncertainty-Based Evaluation

Probabilistic evaluation methods extend deterministic assessment by explicitly representing uncertainty in model predictions. They characterize predictive behavior through ensembles generated by parameter sampling, alternative forcings, or structural model variants. Uncertainty in hydrological modeling arises from multiple sources, commonly distinguished as aleatory uncertainty (irreducible randomness in natural systems and observations) and epistemic uncertainty (incomplete knowledge of system processes, parameters, or model structure) (Beven, 2016; Kuczera et al., 2007; Kavetski et al., 2006; Li et al., 2022). While this distinction is conceptually clear, practical separation of these uncertainty sources remains challenging, particularly when model residuals exhibit temporal autocorrelation, heteroscedasticity, and non-Gaussian behavior. Formal Bayesian inference frameworks attempt to quantify epistemic uncertainty by estimating posterior parameter distributions using explicit likelihood formulations (Kavetski et al., 2006). These approaches provide a rigorous probabilistic foundation but often rely on assumptions—independent, homoscedastic, normally distributed errors—that are frequently violated in hydrological applications (Schoups & Vrugt, 2010; Mizukami et al., 2019; Smith & Marshall, 2008).

In contrast, informal likelihood approaches such as the Generalized Likelihood Uncertainty Estimation (GLUE) framework embrace equifinality and reject the notion of a unique optimal parameter set (Beven & Binley, 1992; Vrugt et al., 2008; Vrugt et al., 2009; Joseph & Guillaume, 2013). Behavioral filtering based on performance thresholds allows multiple plausible realizations to be retained, emphasizing predictive robustness over optimized fit. However, subjectivity is introduced through model selection further exacerbating uncertainty.

More recently, information-theoretic methods have emerged as a likelihood-free alternative for evaluating predictive information content (Weijs et al., 2010; Jolliffe & Stephenson, 2011). By quantifying mutual information between inputs, simulations, and observations, these approaches establish objective bounds on achievable predictive skill regardless of model formulation. Metrics such as the Ratio of Uncertainty to Mutual Information (RUMI) directly integrate uncertainty magnitude with informational efficiency, providing structural insight that does not depend on residual error assumptions (Pizarro et al., 2025). Despite their conceptual diversity, probabilistic methods often emphasize distributional reliability without directly assessing whether simulated ensemble members reproduce hydrologically meaningful system behavior. As such, probabilistic skill alone does not guarantee physical realism.

### 1.3. Structural and Signature-Based Diagnostics

Structural or signature-based evaluation methods address the assessment of whether models are right for the right reasons (Kirchner, 2006; Zhou et al., 2022; Santos et al., 2018). Signature-based diagnostics evaluate whether simulated time series reproduce key hydrological behaviors embedded in the observed system. Hydrological signatures are metrics or functional representations linked to specific runoff generation processes and system properties. Common examples include flow duration curves, seasonal indices, recession constants, autocorrelation decay rates, and regime-specific exceedance statistics. These diagnostics connect model outputs directly to physical interpretations of storage, persistence, and response dynamics.

Flow Duration Curves (FDCs) are particularly powerful diagnostic tools because different portions of the curve correspond to distinct hydrological processes. High-flow segments reflect rapid runoff responses and storm dynamics, while low-flow tails capture groundwater contributions, storage depletion, and drought persistence. Models that perform similarly under aggregate metrics may exhibit markedly different behavior when evaluated through FDC-based diagnostics (Feng et al., 2020; Shi & Cai, 2024).

Signature-based methods are inherently diagnostic as they do not optimize or rank models but instead reveal how and where simulated behavior diverges from observed hydrological structure. Their interpretability makes them especially valuable for comparative model analysis and for identifying structural deficiencies masked by compensating errors. The value of signature diagnostics is maximized when they are interpreted alongside deterministic and probabilistic assessments.

While these diagnostics capture important aspects of storage, variability, and regime behavior, they do not explicitly test whether simulated discharge reproduces the directional response of the system as flow conditions evolve through time. Hydrological systems exhibit path-dependent behavior arising from the interaction between fast surface pathways and delayed subsurface storage and release processes. As a result, identical discharge magnitudes may correspond to different internal states depending on whether the system is transitioning through rising or receding conditions. This temporal asymmetry manifests as hysteresis between sequential flow states and reflects the memory and routing characteristics of the catchment.

Hysteresis-based diagnostics therefore extend structural evaluation by interrogating aspects of system behavior that are not identifiable from static signatures alone (Muste et al., 2020; Muste et al., 2025; House et al., 2025). They assess whether simulations that reproduce flow magnitudes and distributions also reproduce the timing and storage-release dynamics governing flow evolution. In the context of model evaluation, hysteresis does not provide a measure of predictive accuracy or uncertainty, but functions as a structural test of dynamic consistency, complementing flow-distribution, seasonal, persistence, and regime-conditional diagnostics.

### 1.4. Implications for Evaluation Design

Deterministic, probabilistic, and structural evaluation paradigms address fundamentally different questions about model behavior. Deterministic metrics quantify aggregate predictive agreement, probabilistic methods characterize predictive uncertainty, and structural diagnostics assess behavioral consistency with observed hydrological processes. Results derived from one paradigm cannot be interpreted as substitutes for another, nor can they be meaningfully combined without an explicit analytical structure.

In practice, evaluation studies often apply selected diagnostics independently, with limited attention to how conclusions drawn from different paradigms relate to one another. This separation obscures tradeoffs between accuracy, uncertainty, and behavioral realism and complicates comparative analysis across models, stations, or simulation generations. Identical deterministic performance may coexist with substantially different uncertainty characteristics or structural behaviors, yet such distinctions are difficult to identify without coordinated analysis.

These limitations are not attributable to deficiencies in individual metrics, but rather to the absence of a systematic evaluation structure that preserves paradigm-specific interpretations while enabling their joint analysis. An effective evaluation design must therefore maintain separation between diagnostic layers while allowing results to be interpreted coherently within a single analytical workflow. The methodological implications of such a design form the basis for the HyMES framework described in the methodology section.

### 1.5. Proposed Framework

This study introduces the Hydrological Model Evaluation System (HyMES) as a unified evaluation framework that formalizes deterministic, probabilistic, and structural diagnostics within a coherent analytical structure available through a browser-based client-side web application. HyMES is explicitly model-agnostic and operates as an evaluation layer applied to externally generated simulations and observed discharge records. Its primary contribution is organizing established diagnostic tools into a comprehensive, multi-layer evaluation workflow that preserves interpretability, comparability, and reproducibility.

The framework is demonstrated using retrospective streamflow simulations from multiple versions of the National Water Model evaluated across a network of gauging stations in the New Orleans region of the United States (Hughes et al., 2024; Johnson et al., 2019; Gochis et al., 2020; Cosgrove et al., 2024; Niu et al., 2011; McKay et al., 2012). These applications illustrate how integrated deterministic, probabilistic, and structural diagnostics reveal differences in model behavior that are not evident from single-metric evaluation alone. The remainder of the manuscript describes the conceptual and methodological foundations, analytical structure, and diagnostic components of the HyMES framework, followed by comparative case study results and discussion of implications for hydrological model evaluation practice.

## 2. Methodology

HyMES is a model-agnostic framework designed to support reproducible, multi-layer evaluation of hydrological simulations against observations. The framework treats model evaluation as a post-processing inference task, separating evaluation logic from model generation to enable consistent comparison across physically based, data-driven, and hybrid modeling approaches. The framework provides a unifying structure for deterministic, probabilistic, and structural diagnostics while remaining independent of model architecture, forcing source, and spatial domain.

### 2.1. Framework Architecture

The framework organizes hydrological model evaluation as a set of analytically distinct layers that define how model behavior is assessed across multiple, non-substitutable dimensions. Each layer addresses a specific evaluation question, predictive accuracy, uncertainty behavior, or structural realism, and constrains the interpretation of subsequent diagnostics. This structure preserves traceability between observed data, model simulations, and evaluative conclusions while remaining agnostic to model architecture or data source. The framework separates evaluation into five distinct steps: defining comparable data, establishing temporal consistency, assessing deterministic agreement, characterizing uncertainty, and diagnosing structural behavior.

The *Data Ingestion* component accepts inputs from two pathways: (1) direct retrieval of observational and model output time series from remote services (e.g., USGS via CUAHSI WaterOneFlow and NWM retrospective archives in S3 Amazon Bucket accessed through HydroLang (Erazo et al., 2022; Erazo et al., 2023; Tolson & Shoemaker, 2007; Rafieeinasab et al., 2024), and (2) locally provided simulations and observations. Both pathways feed a common validation and harmonization routine that ensures consistent units, temporal continuity, and metadata integrity.

The *Preprocessing and Alignment* component synchronizes observed and simulated datasets to shared evaluation windows, applying resampling, gap handling, and temporal normalization. This alignment ensures that all diagnostics operate on comparable time series.

The *Deterministic Evaluation* component computes classical performance metrics (e.g., correlation structure, bias ratios, variance ratios, residual-based errors), generating the first quantitative assessment of agreement while retaining residuals for downstream analysis.

The *Probabilistic Evaluation* component extends deterministic assessment to ensemble or parameter-sampled simulations, enabling evaluation of coverage, sharpness, likelihood consistency, posterior behavior, and distributional robustness. Ensemble outputs at this stage support uncertainty envelopes, metric distributions, and likelihood-based comparisons.

The *Structural Diagnostic* component evaluates physically interpretable signatures of hydrological behavior, including flow-regime structure (FDC metrics), persistence and autocorrelation characteristics, seasonal organization, and hysteretic dynamic response. These diagnostics assess whether simulations reproduce key features of observed catchment behavior beyond aggregate predictive accuracy. Figure 1 provides an overview of this multi-layer evaluation architecture.

HyMES is delivered as a browser-based application executing the full workflow in the client environment written in TypeScript. Statistical routines are computed locally using WebR (WebR, 2025; Bengtsson, 2025; Paredes, 2025; Stagg, 2023). R language scripts compiled to WebAssembly, ensuring reproducible numerical behavior across operating systems, zero-installation portability, and full transparency of analytical steps. To support ensemble-based and resampling-intensive diagnostics, HyMES uses HydroCompute (Erazo et al., 2024), a lightweight orchestration layer that coordinates a pool of Web Worker threads. Per-station metric computation, ensemble evaluation, resampling, and structural signature extraction are decomposed into independent units and executed asynchronously. Task dependencies preserve the evaluation hierarchy, ensuring deterministic outputs become available before probabilistic and structural diagnostics are interpreted. Intermediate results stream back incrementally, enabling real-time updates when the user modifies the evaluation period, conditioning thresholds, or diagnostic selection. Figure 1 shows the schematic architecture of the proposed evaluation framework, and Figure 2 shows the map and dashboard views of the platform.

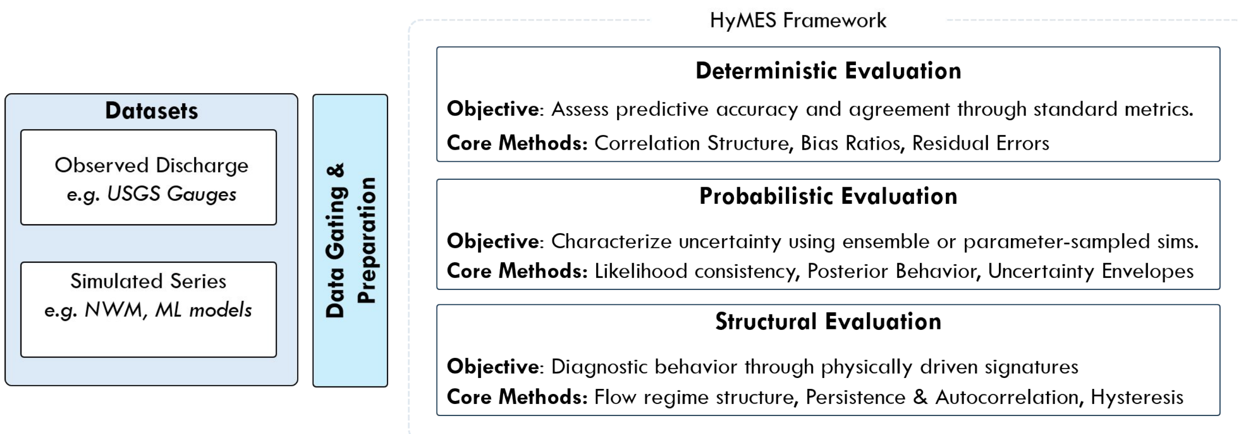


Figure 1. Architecture of the HyMES framework and web app.

## 2.2. Deterministic Evaluation and Error Characterization

Deterministic evaluation establishes baseline agreement between simulated and observed discharge and defines the error structure on which all subsequent analyses depend. This evaluation layer treats performance metrics and residuals as statistical objects, not summary scores, and explicitly distinguishes accuracy, bias, and temporal organization of error. All deterministic diagnostics are computed independently at the station level using temporally aligned observed and simulated discharge records. Temporal alignment, unit consistency, and treatment of missing data are held fixed across simulations to ensure that all metrics are conditioned on identical information. From here onwards, let $Q_t^{obs}$ denote observed discharge and $Q_t^{sim}$ denote simulated discharge at time $t = 1,\ldots,T$.

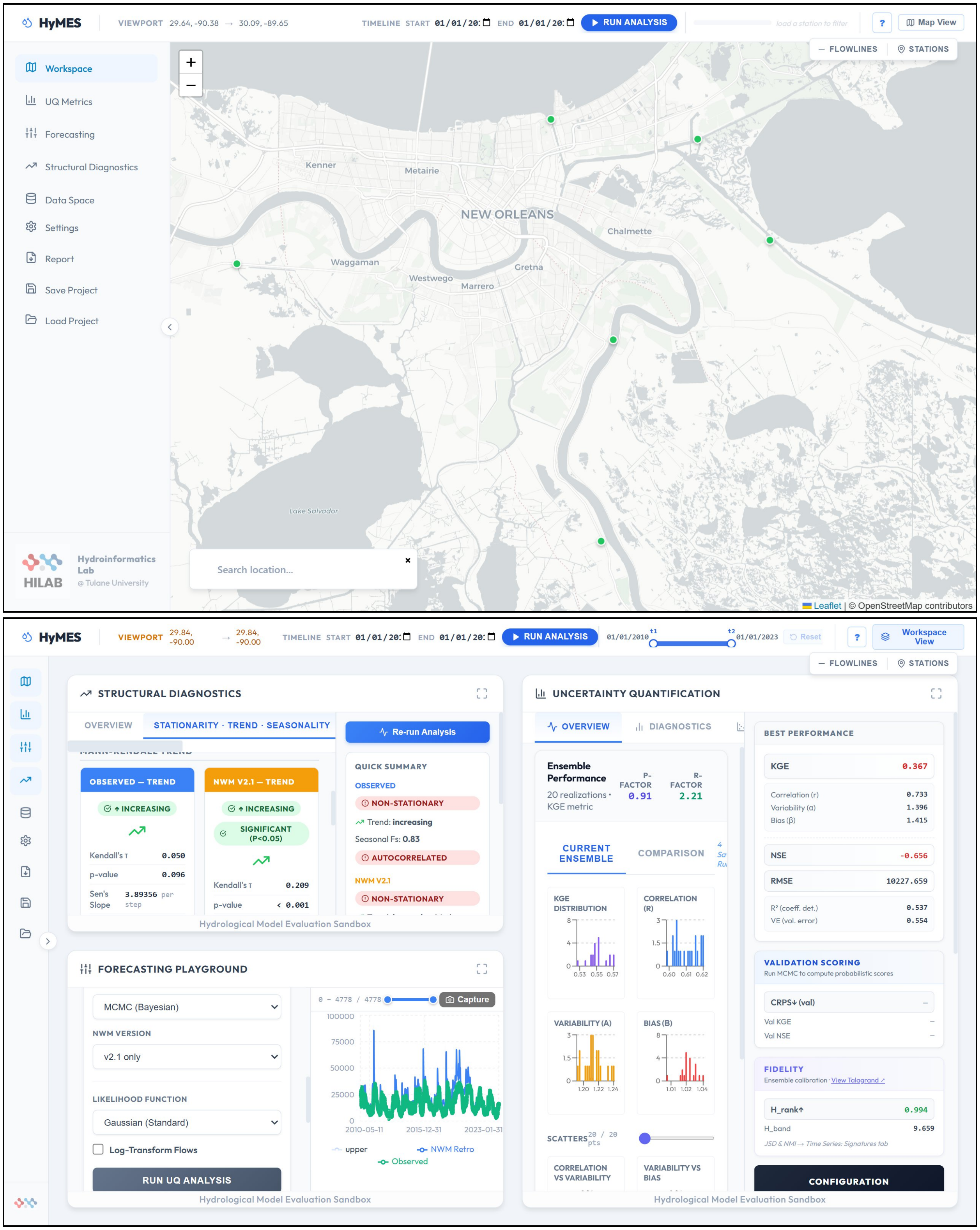

Figure 2. Overview of the user interface of the HyMES web application. The interactivity within the browser enables analysis directly in browser. Each window contains specific analytical

outputs bound to the type of epistemic analysis done. The windows also contain within their sidebars an AI assistant that synthesizes data from an expert perspective.

### 2.2.1. Evaluation Objectives

Deterministic evaluation addresses three non-substitutable questions: i) Predictive agreement: Does the simulation reproduce observed discharge magnitude and timing? ii) Volumetric consistency: Does the simulation conserve water mass over the evaluation period? iii) Error organization: How are discrepancies structured across time and flow regimes? No single metric answers all three questions. Deterministic evaluation therefore combines complementary diagnostics and preserves the full residual time series.

### 2.2.2. Efficiency-Based Performance Metrics

Efficiency metrics quantify predictive agreement relative to benchmark behavior derived from observations. NSE evaluates squared error normalized by observed variance (Eq. 1):

$$\mathrm{NSE} = 1 - \frac{\sum_{t=1}^{T} (Q_t^{sim} - Q_t^{obs})^2}{\sum_{t=1}^{T} (Q_t^{obs} - \overline{Q^{obs}})^2}. \qquad \text{Eq. 1}$$

NSE emphasizes high-flow periods and provides limited insight into the source of disagreement. The KGE decomposes performance into correlation, variability, and bias components (Eq. 2):

$$\mathrm{KGE} = 1 - \sqrt{(r-1)^2 + (\alpha-1)^2 + (\beta-1)^2}, \qquad \text{Eq. 2}$$

where r is the Pearson correlation coefficient, $\alpha = \sigma_{sim}/\sigma_{obs}$ represents relative variability, and $\beta = \mu_{sim}/\mu_{obs}$ represents mean bias. KGE is retained as a vector diagnostic. Its components are interpreted independently to attribute performance loss to timing errors, variance distortion, or systematic bias.

### 2.2.3. Error-Magnitude Metrics

Error-magnitude metrics quantify absolute discrepancy without normalization by observed variance. The Root Mean Square Error (RMSE) penalizes large residuals and is sensitive to peak-flow errors (Eq. 3).

$$\mathrm{RMSE} = \sqrt{\frac{1}{T}\sum_{t=1}^{T} (Q_t^{sim} - Q_t^{obs})^2} \qquad \text{Eq. 3}$$

The Mean Absolute Error (MAE) provides a robust complement less influenced by extremes. These metrics are interpreted jointly with efficiency measures to distinguish variance-dominated error from persistent bias (Eq. 4).

$$\mathrm{MAE} = \frac{1}{T}\sum_{t=1}^{T} |\, Q_t^{sim} - Q_t^{obs} \,| \qquad \text{Eq. 4}$$

### 2.2.4. Volumetric Consistency and Water Balance

Hydrological realism requires consistency of long-term fluxes. A simulation may reproduce short-term dynamics while accumulating volumetric error. Percent Bias (PBIAS) quantifies systematic over- or under-prediction, while the Water Balance Error (WBE) provides a normalized cumulative comparison (Eq. 5). Volumetric diagnostics isolate mass-balance discrepancies that may remain undetected by efficiency-based metrics.

$$\begin{aligned} \mathrm{PBIAS} &= 100 \times \frac{\sum_{t=1}^{T} (Q_t^{sim} - Q_t^{obs})}{\sum_{t=1}^{T} Q_t^{obs}} \\ \mathrm{WBE} &= \frac{\sum_{t=1}^{T} Q_t^{sim} - \sum_{t=1}^{T} Q_t^{obs}}{\sum_{t=1}^{T} Q_t^{obs}}. \end{aligned} \qquad \text{Eq. 5}$$

### 2.2.5. Residual Definition and Preservation

Residuals are defined as $\varepsilon_t = Q_t^{sim} - Q_t^{obs}$ and are preserved explicitly and treated as primary diagnostic data. Aggregated metrics discard information about heteroscedasticity, temporal dependence, and regime-specific behavior that remains encoded in the residual series. Residual preservation enables: i) bootstrap-based estimation of metric stability; ii) detection of persistence and memory effects; iii) regime-conditional attribution of error; and iv) identification of structural bias change over time. This design establishes a direct analytical link between deterministic evaluation and subsequent probabilistic and structural diagnostics. Deterministic metrics define necessary but incomplete conditions for model adequacy. High efficiency does not imply robustness under uncertainty, and low bias does not imply hydrological credibility. Deterministic evaluation therefore serves as the reference layer against which uncertainty characterization and structural diagnostics are conditioned and interpreted. Formal definitions, metric variants, and sensitivity analyses are documented in Supplementary Materials 1 Section S1.

## 2.3. Probabilistic Evaluation and Uncertainty Characterization

Deterministic evaluation yields point estimates of model performance conditioned on a single realization of model structure, parameters, and forcings. These estimates provide no information about the stability of performance under uncertainty, nor about the distribution of plausible error structures consistent with observed data. Probabilistic evaluation addresses these limitations by explicitly representing simulated discharge and derived performance metrics as random variables induced by uncertainty in the modeling process. The probabilistic analysis in the framework operates on ensembles of simulated discharge generated outside the evaluation framework through parameter perturbation, alternative forcings, or structural variants. Let $Q_t^{(i)}$ denote simulated discharge from ensemble member $i = 1,\dots,N$. The ensemble induces an empirical distribution over discharge trajectories and, by extension, over deterministic performance metrics and residual structures. The objective of this layer is to perform inference to quantify the robustness, calibration, and informational efficiency of deterministic performance under explicitly defined sources of uncertainty.

### 2.3.1. Sampling Distributions of Performance Metrics

Scalar performance metrics conceal both ensemble variability and sampling uncertainty associated with finite record length. Probabilistic evaluation focuses on the sampling distributions of deterministic performance metrics. For a deterministic metric M (e.g., KGE, NSE, RMSE), an ensemble-induced distribution (Eq. 6) is obtained by evaluating each ensemble member against the observed discharge record. This distribution characterizes sensitivity of apparent model skill to uncertainty in parameters, forcings, or structure.

$$\left\{M^{(1)},M^{(2)},\dots,M^{(N)}\right\} \tag{Eq. 6}$$

Bootstrap resampling of paired observed–simulated discharge records is additionally applied to quantify sampling variability independent of ensemble construction. Bootstrap confidence intervals provide a record-length-conditioned uncertainty bound on metric estimates without assuming Gaussian or independent residuals, interpreted as robustness diagnostics, not as probabilistic forecasts of future performance.

### 2.3.2. Conditional Ensemble Definition and Equifinality

Unconditional ensembles often include realizations that are grossly inconsistent with observations and hinder uncertainty interpretation. The framework supports conditional ensemble evaluation, where ensemble members are filtered using explicit deterministic performance criteria. Let $\mathscr{E}$ denote the full ensemble and $\mathscr{E}^* \subset \mathscr{E}$ the subset satisfying a predefined acceptance criterion (e.g., $\mathrm{KGE} \geq \tau$). Analysis of $\mathscr{E}^*$ isolates uncertainty attributable to equifinality among acceptable simulations, instead of conflating it with predictive failure. This conditioning strategy aligns with informal likelihood approaches while retaining transparency through explicit threshold reporting. Threshold selection is treated as an analytical decision and reported for all results.

### 2.3.3. Predictive Distributions and Uncertainty Geometry

For a given ensemble, predictive uncertainty is summarized by empirical quantiles of simulated discharge at each time step $Q_{t,p} = \mathrm{Quantile}_p\left\{Q_t^{(1)},\dots,Q_t^{(N)}\right\}$. These quantiles define time-varying uncertainty envelopes that capture the geometry of ensemble spread. Ensemble width, asymmetry, and temporal coherence are preserved. Uncertainty envelopes are treated as diagnostic objects; they do not imply probabilistic correctness of individual ensemble members and are interpreted comparatively across models and configurations.

#### 2.3.4. Calibration, Sharpness, and Informational Efficiency

Uncertainty representations are evaluated using complementary diagnostics that jointly assess calibration and spread. Coverage probability, defined as the fraction of observed discharge values contained within a specified ensemble envelope, evaluates statistical consistency between ensemble width and observed variability. Ensemble spread, quantified using inter-quantile ranges and entropy-based measures, evaluates sensitivity of predictions to uncertainty in model realization. High coverage accompanied by excessive spread indicates poor informational efficiency, whereas low coverage indicates under-represented uncertainty. These diagnostics distinguish between ensembles that are merely wide and those that are both reliable and sharp. Information-theoretic metrics, including entropy-based measures and mutual information diagnostics, provide an additional evaluation axis by quantifying the degree to which ensemble predictions reduce uncertainty relative to climatological benchmarks.

#### 2.3.5. Role of the Probabilistic Layer

Probabilistic evaluation does not supersede deterministic assessment. It constrains interpretation of deterministic metrics by quantifying their stability, sensitivity, and information content under uncertainty. Structural diagnostics are interpreted conditionally on both deterministic agreement and probabilistic robustness. This layer defines the uncertainty space where questions of hydrological realism and structural consistency are addressed. Formal definitions and estimation procedures are documented in Supplementary Materials 1 Section S2.

### 2.4. Structural and Signature-Based Diagnostics

Deterministic and probabilistic diagnostics quantify predictive agreement and uncertainty but do not test whether simulated discharge reproduces the structural properties of the observed hydrological system. Structural diagnostics evaluate characteristics of streamflow time series that are diagnostic of storage behavior, response timing, persistence, and regime-specific dynamics. These properties are not identifiable from aggregate error metrics or ensemble spread alone.

Structural evaluation is applied conditionally, only simulations exhibiting comparable deterministic performance and acceptable probabilistic robustness are subjected to signature analysis. Under this conditioning, discrepancies in structural diagnostics are interpreted as evidence of behavioral inconsistency, not lack of predictive skill. All structural diagnostics are computed independently at the station level using temporally aligned observed and simulated discharge records.

### 2.4.1. Flow Distribution and Regime Representation

The empirical distribution of discharge reflects the integrated outcome of catchment storage, release, and runoff generation processes. Flow Duration Curves (FDCs) are used to evaluate whether simulations reproduce this distribution across hydrological regimes. For a discharge time series $Q_t$, flows are sorted in descending order and assigned exceedance probabilities $p_i = \frac{i}{T+1}$, where iis the rank and Tthe record length. Observed and simulated FDCs are compared across exceedance intervals corresponding to high-flow, mid-flow, and low-flow regimes. Structural diagnostics derived from FDCs include: a) regime-specific bias in discharge magnitude; b) distortion of distributional slope (flow variability); and c) under- or over-representation of extreme and persistent flows. FDC-based diagnostics evaluate distributional consistency. Simulations with similar KGE or NSE values may nonetheless exhibit distinct FDC behavior, indicating compensatory error structures.

### 2.4.2. Seasonal Organization of Discharge

Seasonal structure reflects the integration of climatic forcing with catchment storage and release processes. Seasonal diagnostics evaluate whether simulations reproduce the timing, amplitude, and persistence of observed seasonal variability. Observed and simulated discharge series are decomposed into seasonal, trend, and residual components using additive time-series decomposition (Eq. 7):

$$Q_t = S_t + T_t + R_t \qquad \text{Eq. 7}$$

Comparisons focus on phase alignment of seasonal peaks, amplitude of seasonal oscillations, and relative contribution of seasonal variance to total variability. Disagreement in seasonal structure identifies deficiencies in forcing integration, evapotranspiration representation, or delayed storage release. These diagnostics distinguish simulations that achieve accurate aggregate performance through timing compensation from those that reproduce seasonal dynamics coherently.

### 2.4.3. Persistence and Memory Structure

Temporal persistence encodes information about catchment storage capacity and recession behavior. Persistence diagnostics evaluate whether simulations reproduce the memory structure of observed discharge. Observed and simulated autocorrelation functions are compared across predefined lag windows. Differences in autocorrelation decay rate and sign structure diagnose excessive smoothing, exaggerated short-term variability, or incorrect recession dynamics. Persistence diagnostics directly interrogate the temporal organization of residuals introduced in results section. Structured residual dependence indicates systematic model deficiencies even when residual variance is small.

#### 2.4.4. Regime-Conditional Performance Attribution

To associate structural discrepancies with predictive consequences, deterministic performance metrics are recomputed conditionally on observed flow regimes. Discharge records are partitioned using quantile thresholds into low-flow, mid-flow, and high-flow classes. Regime-conditional metrics expose compensatory behavior in which strong agreement during stormflow masks persistent errors during baseflow or transitional states. This analysis links structural diagnostics to performance attribution and prevents misinterpretation of aggregate metrics.

#### 2.4.5. Hysteresis Diagnostics and Catchment Memory

Runoff generation in natural catchments reflects the interaction between fast surface pathways and delayed subsurface storage and release processes. This interaction introduces temporal asymmetry between rising and falling limbs of the hydrograph for comparable antecedent flow states. Such asymmetry is not captured by pointwise error metrics, flow distributions, or regime-conditional aggregation, and instead manifests as hysteresis in the temporal organization of discharge. The proposed framework evaluates this behavior using a lagged Q–Q hysteresis diagnostic, which provides a structural test of catchment memory and routing dynamics. The diagnostic assesses whether simulated discharge reproduces the observed directional response of the system during flow increase and recession phases.

The hysteresis diagnostic is constructed by relating discharge at time $t$ to discharge at a previous time $t - k$, forming a closed loop in lagged flow space. The orientation and extent of this loop distinguish rising-limb and falling-limb behavior and encode the degree of temporal memory in the system. To quantify this effect, we define a Hysteresis Index (HI) as the signed area enclosed by the loop, normalized by the squared peak discharge $\mathrm{HI} = \frac{\text{Signed loop area}}{\mathrm{Q_{max}}}$. The sign of the index provides direct physical interpretation. Positive values indicate clockwise hysteresis, consistent with rapid surface runoff or kinematic wave dominance. Negative values indicate counter-clockwise hysteresis, characteristic of delayed subsurface storage and groundwater release. Values near zero indicate weak or symmetric temporal response.

Structural fidelity is evaluated using the hysteresis reproduction error, defined as the difference between observed and simulated hysteresis indices. Small discrepancies indicate minor routing or lag mis-specification, while large discrepancies signal failure to represent dominant runoff generation pathways or storage–release timing. Hysteresis diagnostics are interpreted conditionally alongside deterministic performance and probabilistic robustness. A model may exhibit acceptable aggregate performance and uncertainty behavior while misrepresenting hysteretic structure, indicating compensatory agreement and not necessarily correct internal timing. As such, hysteresis analysis provides a targeted complement to flow-distribution, seasonal, persistence, and regime-conditional diagnostics by explicitly interrogating dynamic catchment memory.

### 2.4.6. Role of Structural Evaluation in the Framework

Structural diagnostics assess whether simulations that appear acceptable under deterministic and probabilistic criteria exhibit hydrologically credible behavior. They evaluate behavioral consistency by testing whether simulated discharge reproduces key structural attributes of the observed system. Structural consistency is therefore interpreted as a necessary condition for model adequacy under uncertainty. Simulations that achieve high deterministic performance yet fail signature-based diagnostics are identified as behaviorally inconsistent, indicating that apparent agreement arises from error compensation.

In this framework, deterministic metrics establish baseline agreement, probabilistic diagnostics constrain robustness, and structural diagnostics provide the final test of behavioral credibility. This layered interpretation prevents over-reliance on any single evaluation paradigm and enables systematic comparison of model behavior across stations, model generations, and modeling approaches. Formal test definitions, regime partitions, scaling choices, and auxiliary structural statistics are documented in Supplementary Material 1 Section S3.

## 2.5. AI-Assisted Diagnostic Interpretation

The multi-layer evaluation framework produces a high-dimensional set of diagnostic outputs spanning predictive accuracy, uncertainty behavior, and structural response. Interpreting these diagnostics consistently, particularly across multiple stations, ensembles, or model configurations, requires substantial domain expertise and often relies on informal, analyst-dependent judgment. The proposed framework introduces an AI-assisted interpretation layer that formalizes expert evaluation reasoning without performing additional statistical inference or modifying computed results. This component operates strictly after all diagnostics have been calculated and consumes only numerical outputs generated by the evaluation framework. Its purpose is to synthesize evidence across layers, attribute dominant deficiencies to hydrologically meaningful causes, and provide concise, actionable feedback to the model evaluator.

Interpretation is organized through a set of expert personas, each corresponding to a well-defined evaluation perspective: deterministic performance, uncertainty robustness, structural and process behavior, and (where applicable) hysteretic catchment memory. Each persona operates on a predefined subset of diagnostics and applies constrained reasoning rules that mirror established hydrological evaluation practice. The AI layer is explicitly bounded, number-driven, and traceable. It is not permitted to introduce external information, invent metrics, or generalize beyond the provided diagnostic context. Final interpretive authority remains with the user; the AI system serves as a structured interpretive scaffold. Table S1 summarizes the diagnostic information provided to the AI interpretation layer, organized by evaluation window and analytical focus. All fields are computed elsewhere in the framework and are provided verbatim to the AI component.

All interpretation is governed by strict constraints. Statements must reference explicit numerical values, avoid generic qualitative claims, and terminate with a single suggested next analytical or modeling step. When external language-model services are unavailable, a deterministic rule-based interpreter applies the same logic to ensure reproducibility. Further description of the AI implementation is found in Supplementary Materials 2.

## 3. Results

For a comprehensive implementation and assessment case study, the HyMES framework was applied to evaluate retrospective streamflow simulations from two versions of the National Water Model (NWM v2.1 and v3.0) across a network of gauging stations located along the Mississippi River and surrounding regions. All analyses were conducted at the station level over a common evaluation period spanning 2010–2023, using consistent preprocessing and diagnostic configurations. The example data can be obtained in the platform.

For each station, HyMES computes the complete suite of deterministic, probabilistic, structural, and hysteretic diagnostics described in method section. Given the high dimensionality of the evaluation space, results are reported selectively. One representative anchor station, USGS 07374525, Mississippi River at Belle Chasse, Louisiana, is examined in detail to illustrate the evaluation workflow and interpretive logic enabled by the framework. Aggregate results across the remaining stations are then summarized to assess generality and scalability.

This section presents a detailed evaluation of the anchor station located along the central Mississippi River. The station serves as a reference example to demonstrate how deterministic, probabilistic, structural, and hysteresis diagnostics are jointly applied and interpreted within the HyMES framework.

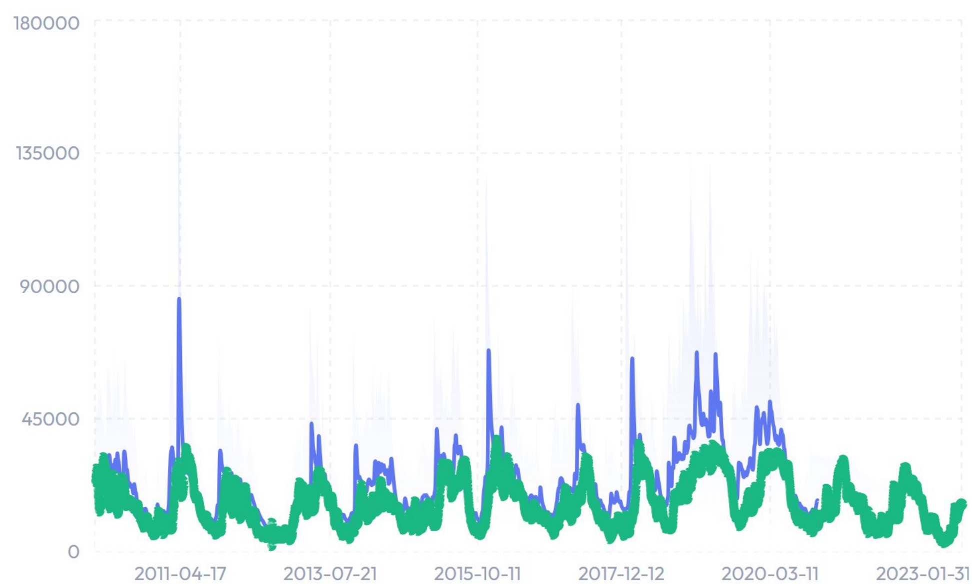


(a)

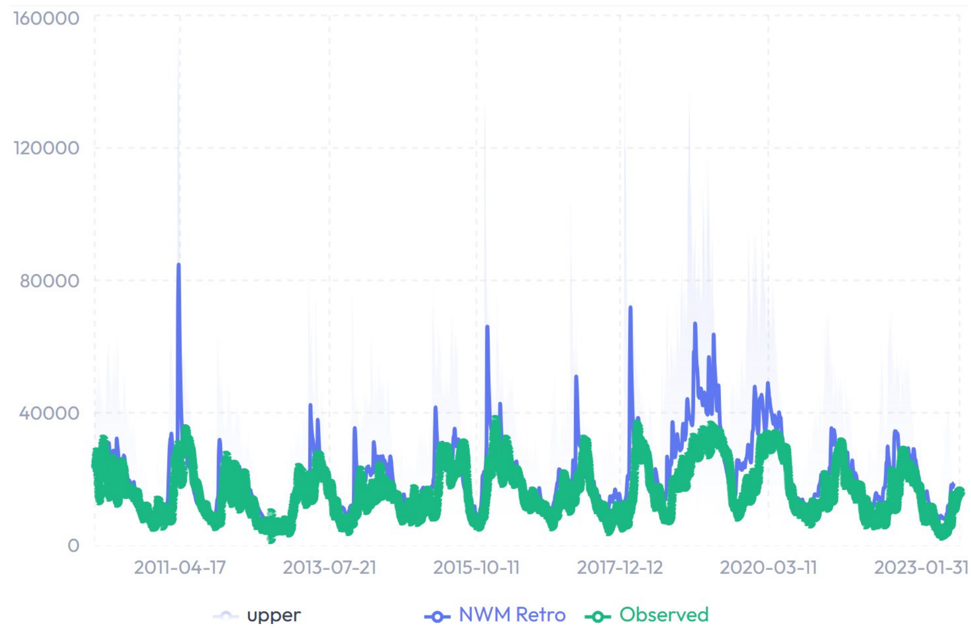


(b)

Figure 3. Figure 3. Comparison of observed discharge with simulated discharge from (a) NWM v2.1 and (b) NWM v3.0 at the anchor station USGS 07374525 (Mississippi River at Belle Chasse, LA). The comparison is based on daily discharge, with discharge reported in m³/s. Note that the NWM v2.1 retrospective simulation terminates at the end of 2020. In both panels, uncertainty envelopes are derived from an ANOVA analysis.

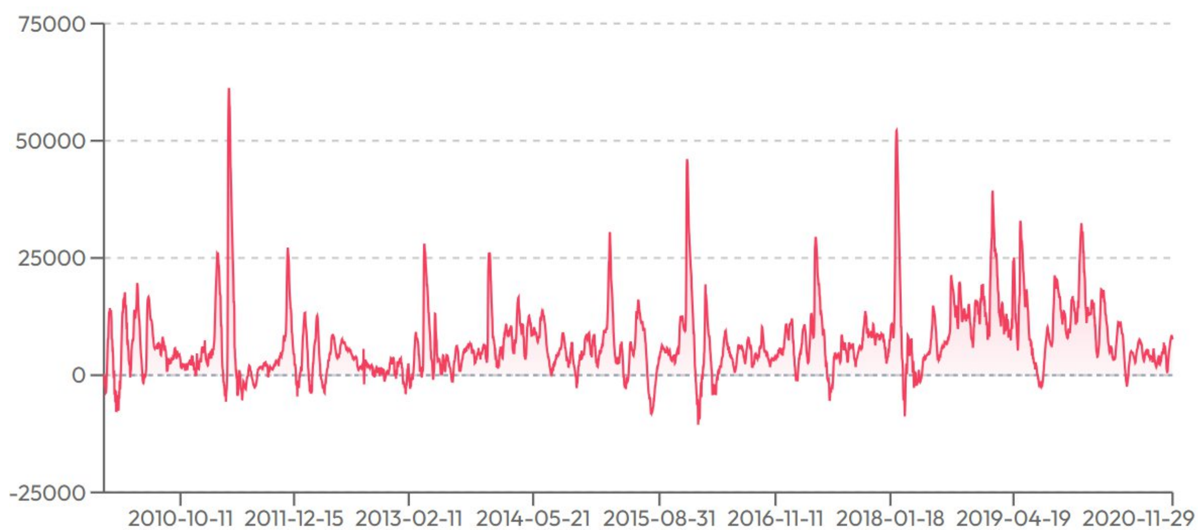


(a)

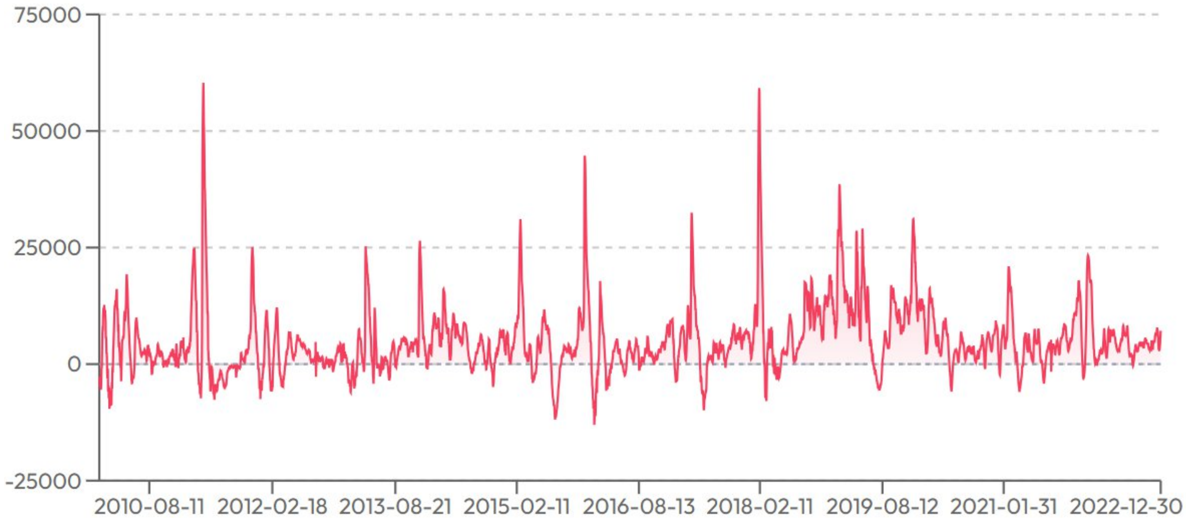


(b)

Figure 4. Corresponding residual bias time series for (a) NWM v2.1 and (b) NWM v3.0, highlighting the magnitude and persistence of systematic error over the evaluation period. It is worth noting the cutoff for the NWM2.1 happens before Dec 2020, while for 3.0 the evaluation period spans all the way until 2023. The analysis herein reflects these discrepancies.

### 3.1. Deterministic Performance

Figures 3–5 and Table 1 summarize deterministic and ensemble-based behavior at the anchor station. Observed and simulated hydrographs (Figure 3) differ in magnitude and timing for both NWM v2.1 and v3.0, and residuals (Figure 4) show persistent bias throughout the evaluation period. Deterministic metrics indicate poor performance in both versions, with negative NSE and KGE values below a mean-flow benchmark. NWM v3.0 reduces error magnitude relative to v2.1, as indicated by lower RMSE and a less negative NSE. However, correlation remains near zero in both versions, indicating weak linear correspondence. Variability ratios ($\alpha \approx 0.43$) indicate reduced flow variability, and both models overestimate mean discharge. The reduction in bias in v3.0 coincides with increased water-balance error. Ensemble distributions (Figure 5) show broad dispersion around simulations that remain inconsistent with observations. These results support extending the evaluation beyond deterministic metrics to probabilistic and structural diagnostics.

Table 1. Deterministic performance metrics for the anchor station.

| **Metric** | **NWM 2.1** | **NWM 3.0** |
|---|---|---|
| RMSE | 13744.92 | 12028.52 |
| R2 | 0.001 | 0.003 |
| Water Balance Error | 0.267 | 0.362 |
| NSE | -2.083 | -1.361 |
| KGE | -0.342 | -0.307 |
| Correlation | -0.024 | -0.057 |

| | | |
|---|---|---|
| Variability | 0.437 | 0.428 |
| Bias | 1.659 | 1.512 |

### 3.2. Probabilistic and Robustness Diagnostics

While deterministic metrics show reduced error magnitude for NWM v3.0 at the anchor station, probabilistic diagnostics assess sensitivity to uncertainty representation. Table 2 summarizes ensemble calibration and sharpness metrics. P-factor values indicate similar nominal coverage for both model versions, but elevated R-factor values show that this coverage is achieved with wide uncertainty intervals. Rank histogram entropy ($H_{\text{rank}}$, normalized Shannon entropy of observation ranks within the ensemble; 1 = perfect uniformity) and uncertainty band entropy ($H_{\text{band}}$, normalized spread of the 95% predictive interval relative to observed variability; lower values indicate tighter, more confident bounds) further differentiate ensemble behavior. Deviations from uniformity indicate biased or overconfident ensembles, with v3.0 exhibiting lower entropy than v2.1. Posterior diagnostics from the MCMC analysis (Table 3) reflect bias correction ($\beta$) and heteroscedastic noise scaling ($\sigma_r$) sampled via DREAM(ZS) to produce calibrated ensemble bounds. Acceptance rates fall below typical ranges, consistent with model–data mismatch or inefficient sampling. Temporal stability of bias was evaluated using the Pettitt change-point test (Table 4), which identifies a statistically significant shift in model bias during the evaluation period. This non-stationarity indicates that full-period metrics may mask time-localized behavior and supports the use of event-scale and structural diagnostics.

Table 2. Ensemble Calibration and Robustness

| Factor | NWM 2.1 | NWM 3.0 |
|---|---|---|
| P-Factor | 0.81 | 0.75 |
| R-Factor | 2.79 | 2.53 |
| Hrank | 0.954 | 0.933 |
| Hband | 9.978 | 9.88 |

Table 3. MCMC Posterior Diagnostics for the selected station.

| Factor | NWM 2.1 | NWM 3.0 |
|---|---|---|
| Mean relative error multiplier | 0.219 | 0.22 |
| Mean bias shift | -0.382 | -0.32 |
| Acceptance rate (15%-45%) | 1.80% | 2.30% |

*Note: The mean relative error multiplier ($\sigma_r$) represents the posterior median of the flow-proportional noise scaling term; values near zero indicate that the model's intrinsic variability closely matches observations, while larger values reflect greater heteroscedastic uncertainty. The mean bias shift (β) is the posterior median multiplicative correction applied to NWM streamflow; negative values indicate systematic model over-prediction. The acceptance rate is the fraction of proposed MCMC parameter draws accepted under the Metropolis–Hastings criterion; the recommended range (15%–45%) reflects efficient posterior exploration — rates well below this* *threshold, as observed here, suggest strong model–data tension or a posterior geometry that is difficult to sample, and should be interpreted alongside convergence diagnostics (see S1).*

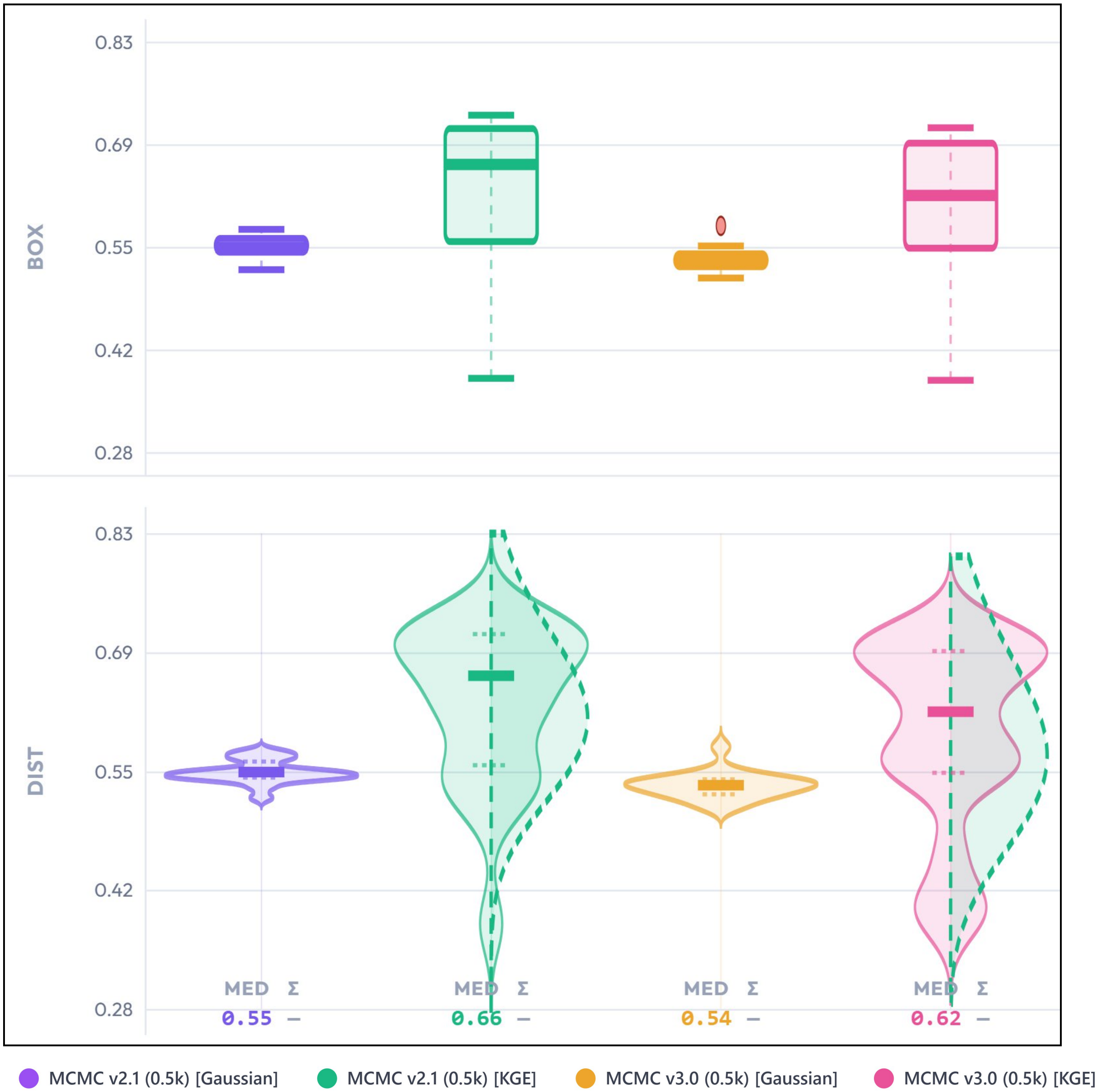


Figure 5. Ensemble performance distributions for four MCMC configurations across KGE realizations. *Upper panel (BOX):* standard box-and-whisker plots where the solid horizontal line denotes the median, box bounds indicate the interquartile range (IQR; 25th–75th percentile), and whiskers extend to 1.5× IQR; points beyond whiskers are plotted as outliers. *Lower panel (DIST):* kernel density estimates (violin plots) of the full posterior predictive distribution, where the profile width at any value reflects the relative density of realizations at that KGE; the embedded solid line marks the median and dotted lines mark the 25th and 75th percentiles. Where two violins overlap (e.g., MCMC v3.0 [KGE]), the dashed contour corresponds to the

overlapping run for visual separation. MED = posterior median KGE; Σ = standard deviation of the realization distribution (shown where available). Colors correspond to NWM version and likelihood function: purple = v2.1 Gaussian; green = v2.1 KGE; orange = v3.0 Gaussian; pink = v3.0 KGE. All runs use 0.5k MCMC iterations.

### 3.3. Structural Diagnostics and Hysteresis Analysis

Table 5 and Figure 6 shows that observed and simulated discharge are non-stationary, with both NWM versions reproducing trend direction but substantially amplifying trend magnitude, particularly in v2.1. While v3.0 reduces this amplification relative to v2.1, both models exhibit stronger persistence and variance growth than observed, indicating damped short-term variability alongside amplified long-term trends. Table 6 indicates partial distributional improvement in v3.0, with reduced median flow bias and lower Jensen–Shannon divergence. However, both versions remain structurally deficient, exhibiting damped flow variability (FDC slope ratios < 1), weak information overlap (low NMI), and similar aggregate persistence metrics despite differing error structures (ACF scores), suggesting that apparent structural gains arise from compensatory behavior rather than coherent reproduction of observed dynamics. Figure 7 shows the density distribution of both the versions of the NWM and the observed for the anchor station, that highlights the minor discrepancy between the structural elements in information distribution across each model. This is also observed in the summary of non-linearity parity on the JS Divergence in Table 6.

Table 4. Pettit test results.

| Value | NWM 2.1 | NWM3.0 |
|---|---|---|
| Significance | Significant | Significant |
| Change Point | 5/17/2017 | 5/20/2017 |
| P-Value | <1e-12 | <1e-12 |
| Mean Bias Before/After | 43% / 60.9% | 29.3% / 48.3% |

*Note: The Pettitt test is a non-parametric test for an abrupt shift in the central tendency of a time series; a significant result ($p < 0.05$) indicates that model bias is not stationary over the evaluation period. The change-point date marks the identified transition; mean bias before and after the change point (expressed as mean absolute percent error) quantify the magnitude of this shift. Large increases in bias after the change point suggest the model's structural errors intensify under specific hydrologic conditions (e.g., post-spring peak recession), which may not be captured by full-period aggregate metrics. Full distributional diagnostics are reported in S1.*

Table 5. Trend and Stationarity Diagnostics for the Anchor Station.

| Metric | Observed | NWM 2.1 | NWM 3.0 |
|---|---|---|---|
| Stationarity Class | Non-Stationary | Non-Stationary | Non-Stationary |
| AR(1) Coeff. | 0.996 | 1 | 1 |
| Variance ratio | 1.599 | 2.182 | 1.72 |

| Metric | Observed | NWM 2.1 | NWM 3.0 |
|---|---|---|---|
| Mann-Kendall trend | Increasing | Increasing | Increasing |
| p-value | 0.096 | <0.001 | <0.001 |
| Kendall's T | 0.05 | 0.209 | 0.117 |
| Sen's Slope | 3.893 | 21.964 | 10.575 |

*Note: The AR(1) coefficient measures first-order temporal autocorrelation; values at or near 1 indicate near-unit-root behavior (persistence), suggesting the series has no tendency to revert to a long-run mean and is consistent with non-stationarity. The variance ratio compares the variance of the second half of the record to the first; values above 1 indicate increasing variance over time. The Mann-Kendall test is a non-parametric test for monotonic trend; a significant p-value (< 0.05) confirms a systematic directional change, with Kendall's τ indicating trend strength (0 = no trend, ±1 = perfect monotonic trend). Sen's slope estimates the median rate of change per unit time in the original units ($m^3$/s/year); the substantially steeper slopes in both NWM versions relative to observations indicate that both models amplify the observed long-term trend, a potential structural bias. A detailed description of all stationarity indicators and their recommended interpretation ranges is provided in S1.*

Table 6. Distributional and seasonal signature at the anchor station.

| Metric | NWM 2.1 | NWM 3.0 |
|---|---|---|
| FDC Slope Ratio | 0.837 | 0.858 |
| Q50 Ratio | 1.453 | 1.299 |
| FDC Score | 0.84 | 0.86 |
| Autocorrelation | Significant | Significant |
| ACF Score | 0.8 | 0.8 |
| Jensen-Shannon Divergence (ideal = 0) | 0.144 | 0.103 |
| Normalized Mutual Information (Ideal = 1) | 0.260 | 0.239 |

*Note: The FDC slope ratio compares the mid-range slope of the simulated to observed flow duration curve; values below 1 indicate that the model underestimates streamflow variability across exceedance probabilities. The Q50 ratio is the ratio of simulated to observed median flow; values above 1 confirm systematic over-prediction of typical flows. The FDC score and ACF score are composite agreement indices (0–1; 1 = perfect); significant autocorrelation indicates that model residuals are temporally correlated, violating independence assumptions and inflating apparent skill. Jensen-Shannon Divergence (JSD) measures the information-theoretic distance between simulated and observed flow distributions (0 = identical distributions; 1 = maximally different); Normalized Mutual Information (NMI) quantifies shared information between the two series (1 = perfect dependence; 0 = independence). The low NMI values here indicate that NWM captures only a limited portion of the observed flow variability structure despite reasonable aggregate metrics.*


Figure 6. Reliability diagrams showing rank histogram distributions comparing observed streamflow against ensemble predictions from (a) NWM v2.1 (top) and (b) NWM v3.0 (bottom). Each bar represents the frequency of observations falling within a given rank bin (0–10% through 100–110%) across the ensemble; a perfectly reliable ensemble produces a uniform distribution matching the red dashed reference line ("Perfect Reliability"). Bars shaded orange indicate over-represented bins (frequency exceeding 50% above expected), reflecting systematic ensemble under-dispersion or directional bias at those ranks; green bars fall within 50% of the expected uniform frequency. The dispersion statistic ($\chi^2$) quantifies overall departure from uniformity — larger values indicate greater unreliability; values of 1015.7 (v2.1) and 4002.0 (v3.0) both indicate significant over-dispersion (Under/Over-dispersed), with the pronounced spike at the 0–10% rank bin in both panels reflecting persistent ensemble over-prediction relative to observations.

**Hysteresis Behavior:** Hysteresis diagnostics evaluated dynamic catchment memory using lagged Q–Q analysis. A well-isolated high-flow event on March 31, 2011, was identified using a 21-day window capturing the full rising limb, peak, and recession (Table 7, Figures 8 and 9). At the anchor station, observed discharge exhibits counter-clockwise hysteresis, characteristic of baseflow-dominated response. Both NWM v2.1 and v3.0 reproduce the loop orientation and show small hysteresis reproduction errors ($|\Delta HI| \approx 0.002–0.01$), indicating agreement in lagged flow response despite poor deterministic performance. This result demonstrates that simulated discharge may reproduce dynamic catchment memory even when aggregate accuracy and uncertainty diagnostics indicate compensatory behavior.

**AI-Assisted Interpretation:** For the anchor station, the AI interpretation synthesizes diagnostics across evaluation layers. For both NWM v2.1 and v3.0, it identifies reduced flow variability, persistent positive bias, and limited ensemble robustness. Differences between model versions are reflected in distributional metrics, with v3.0 showing reduced median bias but similar variability damping and weak probabilistic calibration. Hysteresis diagnostics are retained in the synthesis, with both models reproducing loop orientation and event-scale lag structure. These features are identified alongside discrepancies in deterministic and probabilistic metrics, indicating divergence between dynamic response characteristics and aggregate performance.

The AI-generated summaries consolidate these patterns into a single station-level assessment, preserving information from deterministic, probabilistic, structural, and hysteretic diagnostics. Outputs are derived directly from the computed metrics and provide a consistent basis for comparison across model versions. Additional details on the interpretation logic and outputs are provided in the Supplementary Materials 2 Table 6.

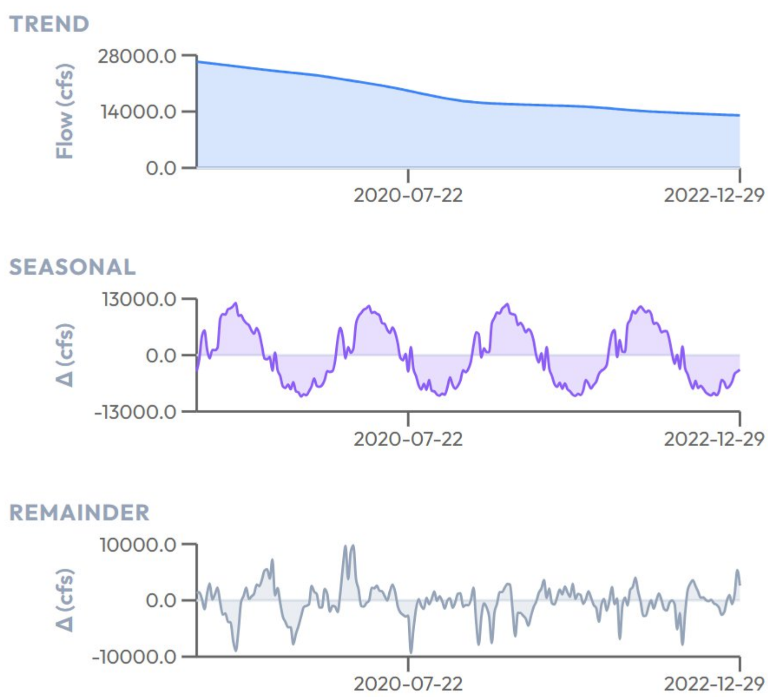


(a)

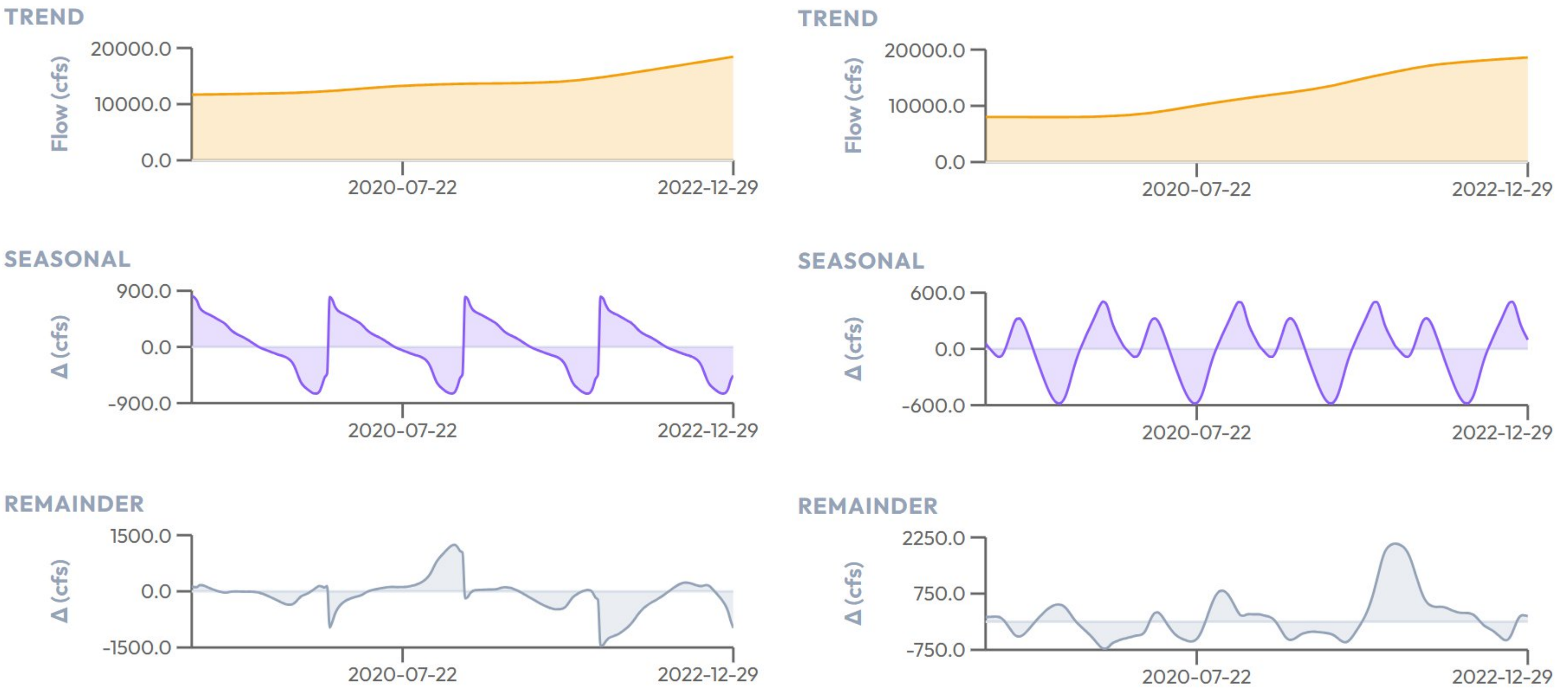


(b) (c)

Figure 7. Seasonal decomposition of (a) observed values with a seasonal strength of 0.83, (b) NWM 2.1 with a seasonal strength of 0.09 and (c) NWM 3.0 with a seasonal strength of 0.24.

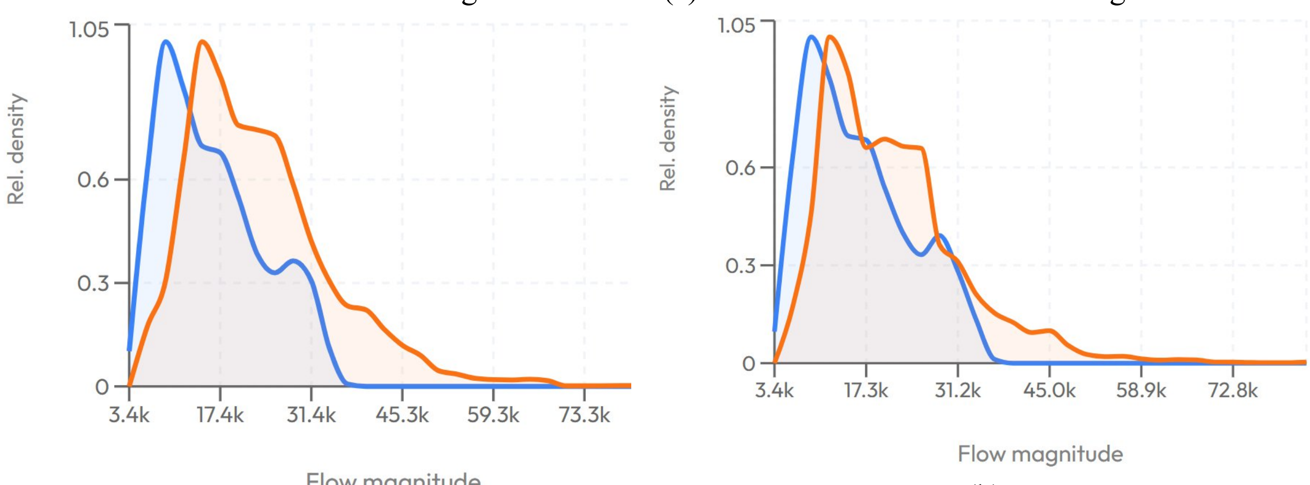


(b)

(a)

Figure 8. Flow frequency distributions used to calculate the Jensen-Shannon and information criterion for (a) Observed vs NWM 2.1. and (b) Observed vs NWM 3.0. The blue line represents observations, and the orange line represents the models.

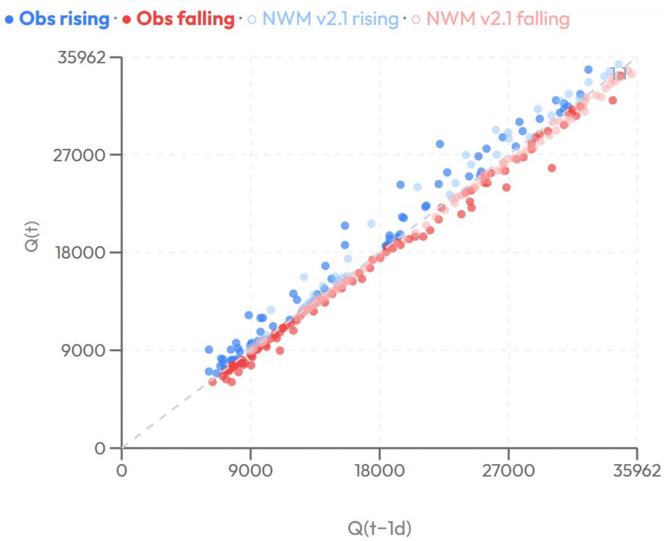
• Obs rising · • Obs falling · ○ NWM v2.1 rising · ○ NWM v2.1 falling
Q(t)
Q(t−1d)
35962
27000
18000
9000
0
1:1

(a)

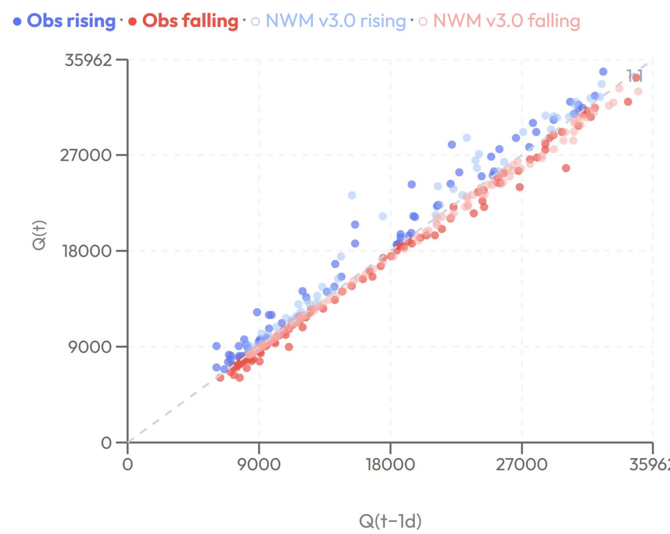
• Obs rising · • Obs falling · ○ NWM v3.0 rising · ○ NWM v3.0 falling
Q(t)
Q(t−1d)
35962
27000
18000
9000
0
1:1

(e)

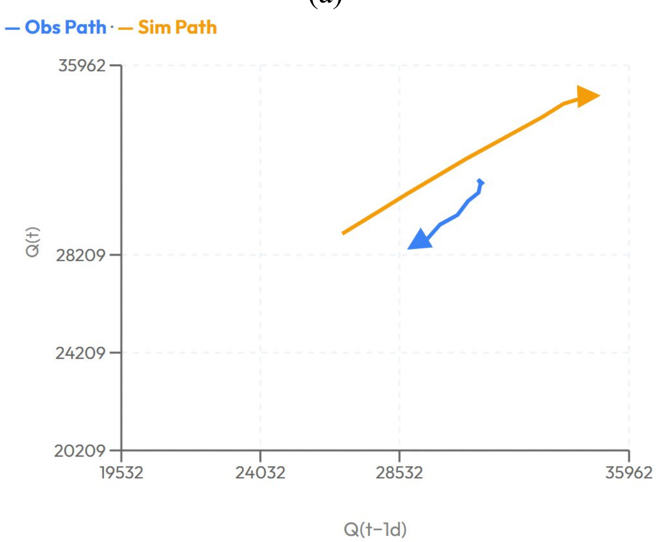
— Obs Path · — Sim Path
Q(t)
Q(t−1d)
35962
28209
24209
20209
19532
24032
28532

(b)

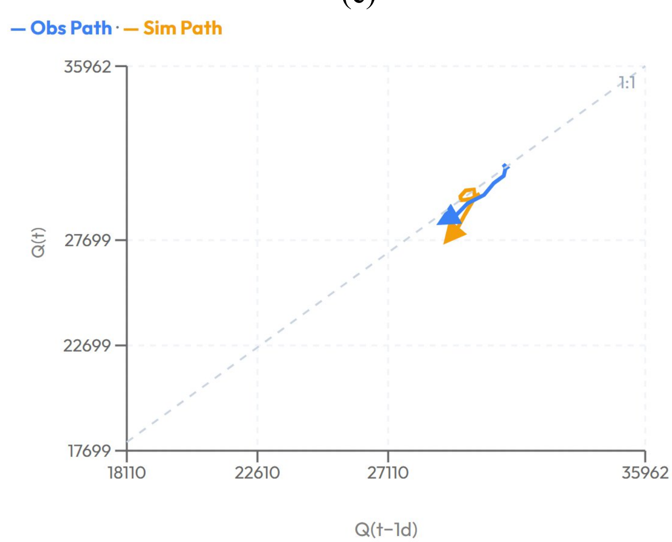
— Obs Path · — Sim Path
Q(t)
Q(t−1d)
35962
27699
22699
17699
18110
22610
27110
1:1

(f)

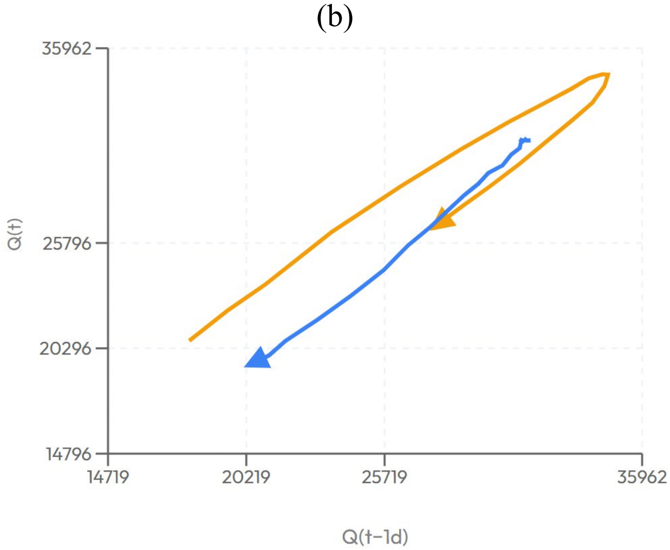
Q(t)
Q(t−1d)
35962
25796
20296
14796
14719
20219
25719

(c)

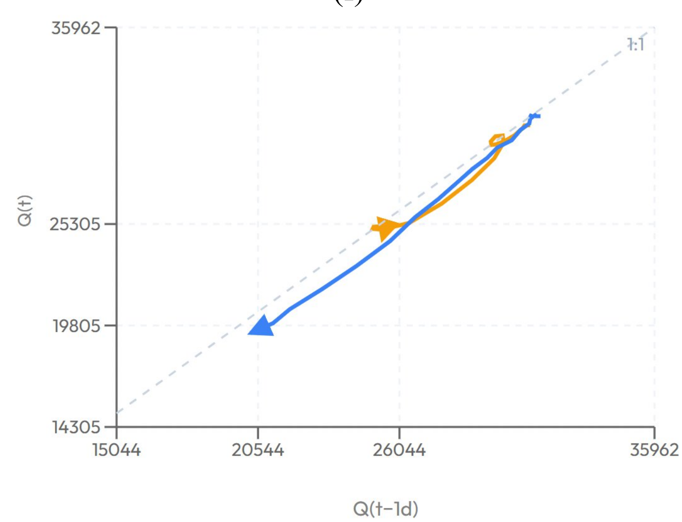
Q(t)
Q(t−1d)
35962
25305
19805
14305
15044
20544
26044
1:1

(g)

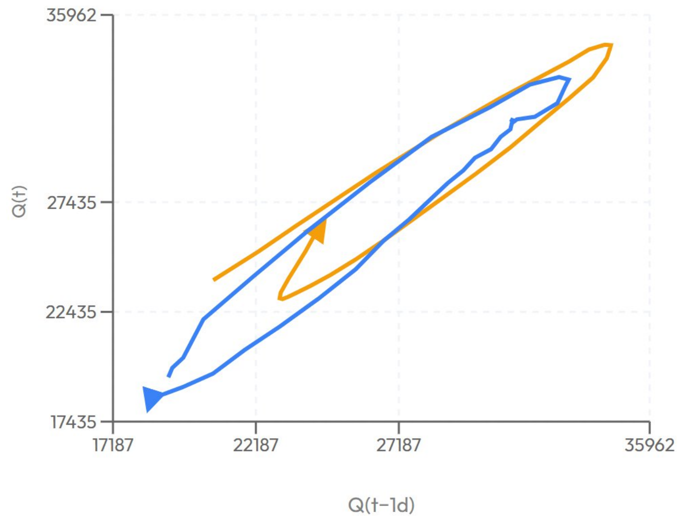


(d)

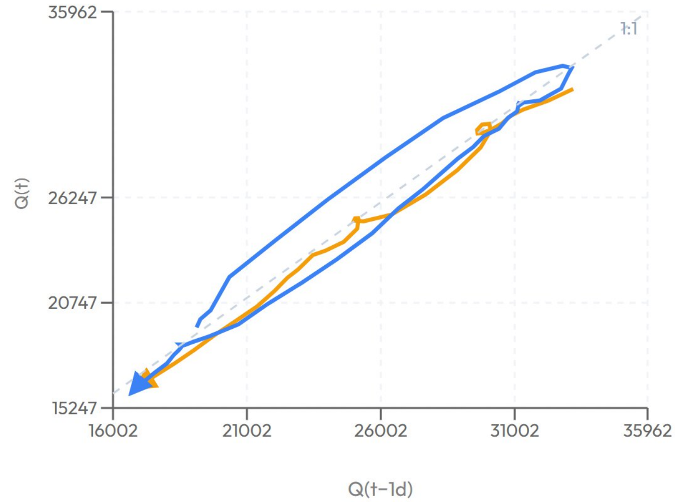


(h)

Figure 9. Observed and simulated hysteretic behavior for the high-flow event of March 31, 2011 at the anchor station. Panels show lagged Q–Q hysteresis loops comparing (a-d) observations and NWM v2.1, and (e-h) observations and NWM v3.0 at a lag of one day. Panels illustrate the evolution of simulated hysteresis geometry for NWM v3.0 at increasing lag times of 11, 22, and 60 days, respectively, highlighting changes in loop orientation and extent with lag length.

Table 7. Hysteresis diagnostics for the event of April 11, 2011. The HI for the observed station was -0.0123 at 60 days. The values are calculated at a window of 60 with a lag of 1 day.

| Evaluation Metric | NWM 2.1 | NWM 3.0 |
|---|---|---|
| Simulated HI | -0.011 | -0.004 |
| $\Delta HI = HI_{obs} - HI_{sim}$ | -0.0112 | -0.0083 |
| Dominant hysteresis interpretation (clockwise / counter-clockwise) | Counter Clockwise | Counter Clockwise |
| Agreement flag (qualitative: agree / mismatch) | Minor Divergence | Minor Divergence |

### 3.4. Aggregated Results Across Remaining Stations

Across the remaining stations, aggregated diagnostics show that the patterns observed at the anchor station are consistent at regional scale summarized in Tables 8, 9 and Figure 10. While NWM v3.0 exhibits modest improvements in deterministic error metrics, structural and probabilistic diagnostics reveal persistent, damped variability, bias, and limited robustness at many stations, indicating that gains are often compensatory.

Table 8. Stations near to the anchor station with different flow regimes and outputs from the NWM.

| Station | Name | Start | End | Mean Discharge ($m^3/s$) |
|---|---|---|---|---|
| A | Bayou Dupre Sector Gate near Violet, LA | 3/9/2017 | 1/1/2023 | 0.02 |
| B | Inner Harbor Navigation Canal nr Seabrook bridge | 8/3/2017 | 1/1/2023 | 0.03 |
| C | GIWW East Storm Surge Barrier at New Orleans, LA | 1/1/2018 | 1/1/2019 | 0.02 |
| D | Naomi Diversion Canal near Naomi, LA | 1/1/2010 | 10/29/2020 | 22.16 |
| E | Davis Pond Freshwater Diversion near Boutte, LA | 1/1/2010 | 1/1/2023 | 0.55 |

Table 9. Aggregated structural, uncertainty, and hysteresis diagnostics across all evaluated stations.

| **NWM 2.1** | | | | | | | |
|---|---|---|---|---|---|---|---|
| Station | P factor | R factor | Hrank | FDC Score | Q50ratio | DHI | Divergence |
| A | 0.03 | 101.07 | 0.023 | 0.66 | 31.911 | 0.0274 | Minor |
| B | 0.6 | 8.44 | 0.595 | 0.58 | 1.624 | -0.0045 | None |
| C | 0.61 | 4.41 | 0.623 | 0.54 | 3.363 | 0.0176 | Minor |
| D | 0 | 0.09 | 0.004 | 0.88 | 0.013 | 0.0726 | Significant |
| E | 0.21 | 1.19 | 0.521 | 0.19 | 0.26 | 0.0356 | Significant |
| **NWM 3.0** | | | | | | | |
| | P factor | R factor | Hrank | FDC Score | Q50ratio | DHI | Divergence |
| A | 0.12 | 71.91 | 0.082 | 0.59 | 27.231 | 0.0372 | Significant |
| B | 0.53 | 2.07 | 0.856 | 0.82 | 1.218 | 0.1427 | Significant |
| C | 0.64 | 3.5 | 0.705 | 0.58 | 3.363 | 0.0108 | Minor |
| D | 0.03 | 0.32 | 0.155 | 0.69 | 0.015 | 0.1186 | Significant |
| E | 0.16 | 1.07 | 0.472 | 0 | 0.225 | 0.0244 | Minor |

### 3.5. Summary of Case Study Findings

Across all evaluated stations, the multi-layer diagnostics reveal that performance differences between NWM v2.1 and v3.0 are heterogeneous and largely compensatory following what the literature has found (Putman et al., 2024; Duan et al., 2023; Yucel et al., 2015; Shortridge et al., 2016). For NWM v2.1, ensemble coverage is highly inconsistent, with many stations achieving low P-factor values only through extremely wide uncertainty bands (high R-factors) and poor calibration (low $H_{rank}$), indicating limited robustness. Structural diagnostics show widespread damped variability and severe median flow bias at several stations, while hysteresis divergence varies from minor to significant, reflecting inconsistent reproduction of dynamic catchment memory. NWM v3.0 exhibits localized improvements, including reduced uncertainty spread and higher rank entropy at selected stations, along with modest gains in distributional metrics. However, these improvements do not generalize across the network, as several stations show continued or increased hysteresis divergence and persistent structural deficiencies, and further climatological and regionalized analysis are needed. Nonetheless, this confirms that apparent progress at individual sites or metrics does not translate into systematic improvement without integrated, multi-layer evaluation.

## 4. Discussions and Limitations

This study presents HyMES as a structured framework for hydrological model evaluation that integrates deterministic accuracy, uncertainty behavior, and structural realism into a single analytical scope. The results demonstrate that applying these layers jointly reveals aspects of model behavior that are not identifiable through aggregate performance metrics alone. In particular, the case study shows that modest deterministic improvements between model versions frequently reflect compensatory error structures and not coherent gains in robustness or structural fidelity.

At the same time, the results highlight several important limitations and open challenges. Structural diagnostics consistently identified damped variability, biased central tendency, and weak seasonal organization across multiple stations, even where deterministic error metrics improved. Probabilistic diagnostics further showed that uncertainty representations remain unstable and poorly calibrated at many locations, with ensemble coverage often achieved through excessive spread. Hysteresis analysis added a complementary perspective by isolating dynamic catchment memory, demonstrating that some aspects of flow response can be reproduced even when aggregate skill is low. However, these dynamic agreements were not systematic and varied substantially across sites (Di Matteo et al., 2026; Hafen et al., 2022; Price  et al., 2021; Jaeger et al., 2021).

The browser-based implementation of HyMES enables interactive, reproducible evaluation without local installations, making complex diagnostics accessible at scale. Nonetheless, executing full ensemble-based and resampling-intensive analyses in a client-side environment imposes practical limits. Memory availability, task concurrency, and execution time constrain ensemble size and temporal resolution, requiring explicit trade-offs between analytical depth and computational feasibility. These constraints do not invalidate the evaluation logic but shape how it can be applied operationally in large-sample studies (Pursnani et al., 2025; Krajewski et al., 2021).

The AI-assisted interpretation layer proved useful for synthesizing high-dimensional diagnostic outputs into consistent, station-level assessments. However, this component must be treated as an interpretive aid rather than an authoritative evaluator. Even with strict input constraints, numerically grounded prompts, and deterministic fallbacks, language-model outputs remain susceptible to over-generalization and emphasis artifacts. Careful framing, transparency of inputs, and user oversight are therefore essential to ensure that AI-generated interpretations support analytical conclusions.

More broadly, the case study highlights a methodological limitation shared by many evaluation frameworks where station-level diagnostics are sensitive to local hydrological context and may not generalize spatially without explicit regional conditioning. Several structural and probabilistic inconsistencies observed here appear linked to regime-specific behavior that is not captured by uniform evaluation across diverse catchments.

<table>
<tr><th>Model / Station</th><th>A</th><th>B</th><th>C</th><th>D</th><th>E</th></tr>
<tr><td>NWM 2.1</td><td>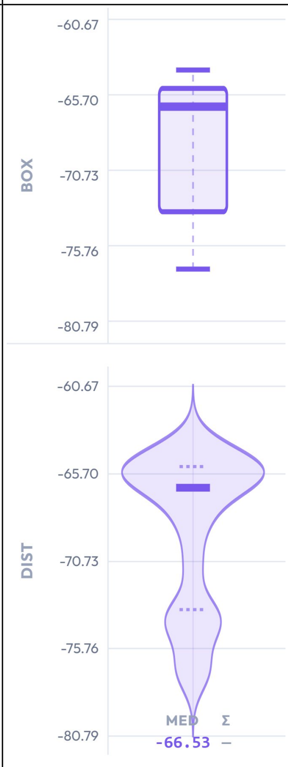
</td><td>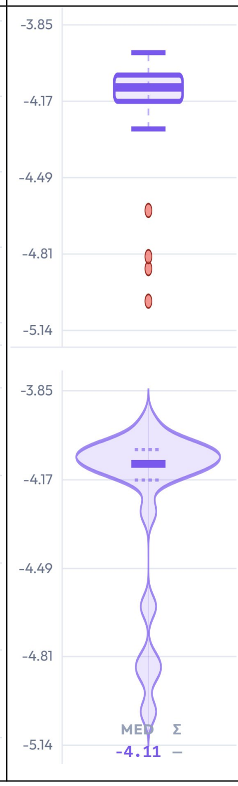
</td><td>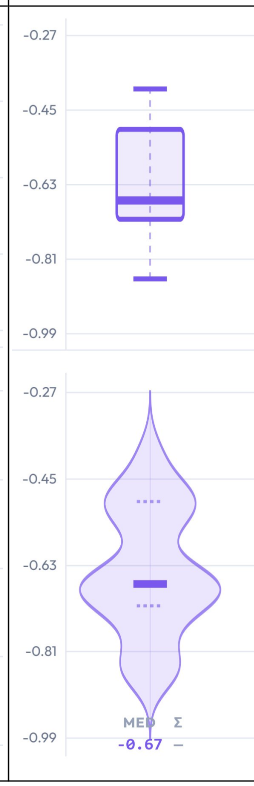
</td><td>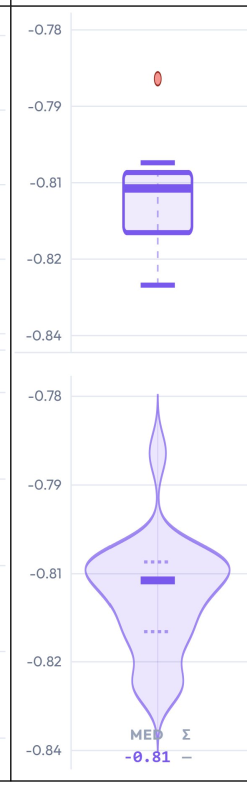
</td><td>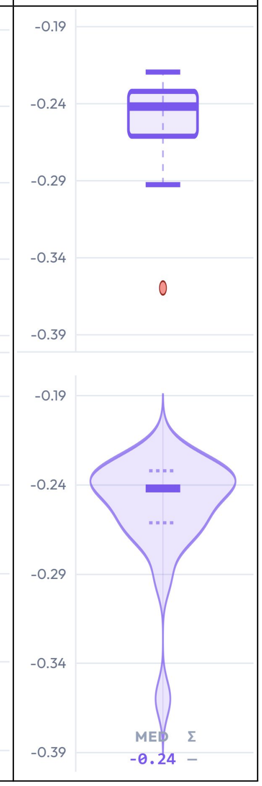
</td></tr>
</table>

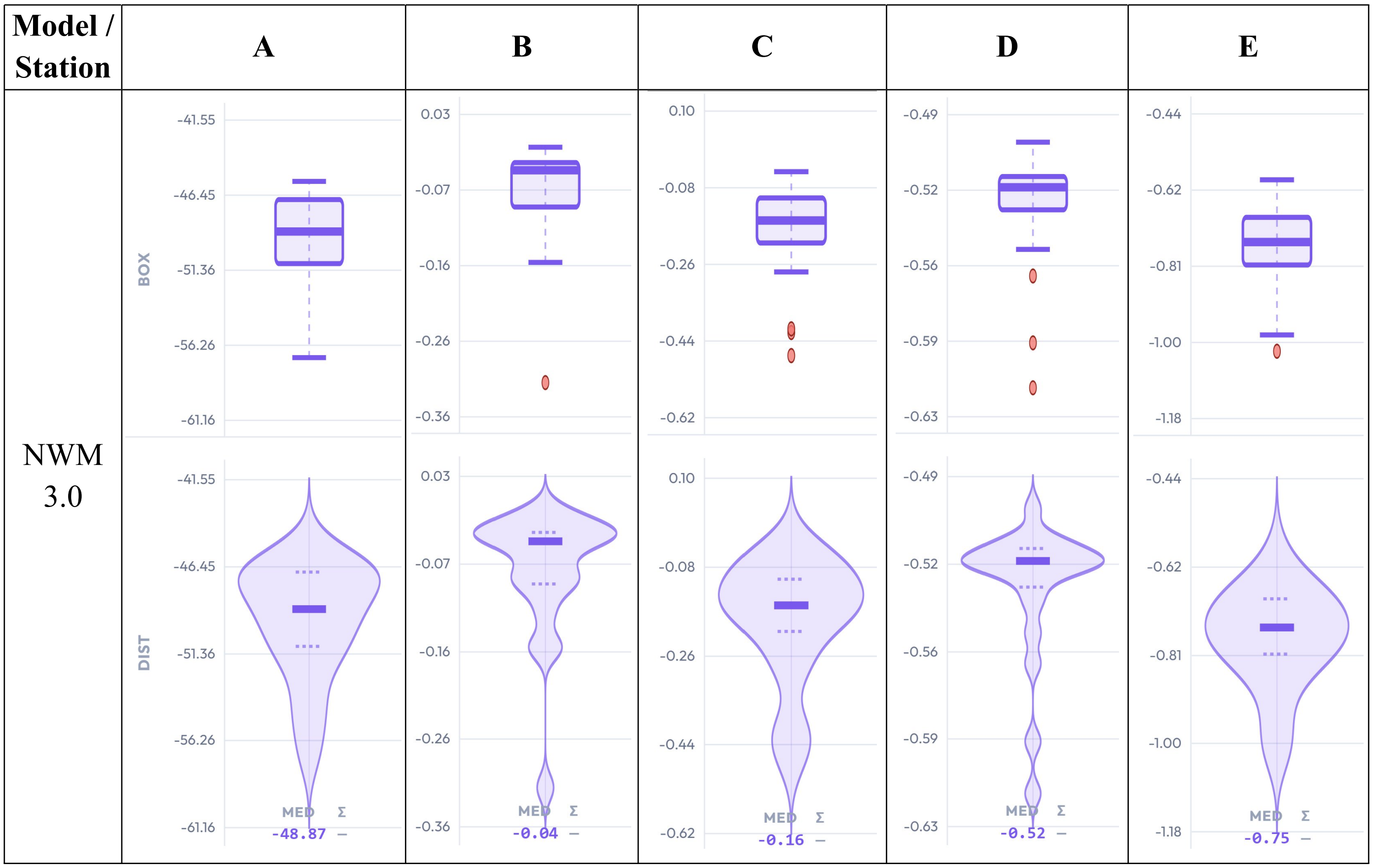


Figure 10. Distributions of 500 ensembles using MCMC for stations A-E for ΔKGE.

## 5. Conclusions

Hydrological model evaluation increasingly requires evidence that extends beyond predictive accuracy. Decisions involving forecasting, operational water management, model development, and scientific inference depend on understanding whether model behavior is reliable, whether uncertainty is appropriately characterized, and whether simulated responses remain consistent with hydrological processes. HyMES addresses this need by providing a comprehensive evaluation framework that integrates deterministic performance, probabilistic behavior, and structural realism within a single, conditionally linked assessment methodology.

Application of the framework to National Water Model v2.1 and v3.0 retrospective simulations demonstrated that improvements in conventional performance metrics can coincide with persistent deficiencies in uncertainty representation, temporal variability, seasonal dynamics, and catchment response. These findings highlight the limitations of evaluation strategies that rely primarily on aggregate deterministic statistics. HyMES resolves these limitations by exposing where predictive agreement results from compensating errors, where uncertainty estimates lack reliability, and where simulated system behavior departs from expected hydrological dynamics.

The framework provides a common evaluation methodology to support stakeholder communities in risk communication and decision support (Islam & Demir, 2026). Model developers can identify structural deficiencies that are not apparent from conventional performance metrics, operational agencies can evaluate model reliability with greater transparency, and researchers can perform reproducible comparisons across model versions, basins, and datasets using a consistent diagnostic framework. The browser-based implementation further lowers barriers to comprehensive evaluation by combining interactive analysis, reproducible workflows, and scalable computation within an accessible environment. The optional AI-assisted interpretation component supports efficient synthesis of diagnostic evidence while preserving expert responsibility for scientific interpretation.

HyMES establishes evaluation as a structured process of evidence integration instead of metric reporting. By making the relationships among deterministic, probabilistic, and structural diagnostics explicit, the framework supports more defensible assessment of hydrological models and provides a foundation for model intercomparison, calibration, benchmarking, and future model development. As hydrological prediction systems continue to increase in complexity and operational importance, evaluation methodologies that characterize both predictive performance and behavioral realism will become essential for developing models that are accurate, reliable, and scientifically credible.

## 6. Future Work

Several directions emerge naturally from the evaluation framework and case study presented here. One important area concerns the incorporation of observation-based physical constraints into model evaluation and interpretation (Sadler et al., 2022; Cho & Kim, 2022; Frame et al., 2020; Downer et al., 2002; Seo et al., 2018). Diagnostics derived from observed seasonality, persistence, storage behavior, and hysteretic response already provide implicit physical information. Formalizing these signals as station-specific constraints could improve how performance metrics are interpreted and used, particularly for distinguishing bias-driven agreement from physically plausible behavior.

A related opportunity lies in extending the evaluation logic toward targeted model refinement and forecasting contexts. While HyMES is designed strictly as an evaluation layer, the structured diagnostics it produces, especially regime-specific and event-scale insights, could inform adaptive weighting, conditional performance assessment, or selective use of model components in forecasting systems. Such use would require careful separation between evaluation and prediction but does not necessitate changes to the underlying framework.

Further work may also explore how evaluation outcomes vary when diagnostics are conditioned on additional observational characteristics, such as hydrological regime, storage dominance, or event type (Di Matteo et al., 2026; Hafen et al., 2022; Price et al., 2021; Jaeger et al., 2021). This would allow evaluation logic to reflect known physical heterogeneity across stations instead of applying uniform criteria across diverse catchments. Finally, the AI-assisted interpretation layer provides a foundation for exploring reproducible evaluation narratives across large station networks and multi-model ensembles. Future work may examine how standardized interpretive logic can be used to support large-sample hydrological studies while preserving traceability between diagnostic evidence and conclusions.

**Acknowledgement:** This material is based upon work supported by the National Science Foundation under Grant No. 2243775 and 2611747. We thank Khoa D. Le for assisting with code integration and testing in this study.

**Declaration of AI-Assisted Technologies**

During the preparation of this work, the authors used ChatGPT to improve the flow of the text, correct any potential grammatical errors, and improve the writing. After using this tool, the authors reviewed and edited the content as needed and took full responsibility for the content of the publication.

## 7. References

Addor, N., Newman, A. J., Mizukami, N., & Clark, M. P. (2020). The CAMELS data set: Catchment attributes and meteorology for large-sample studies. Hydrology and Earth System Sciences, 21(10), 5293-5313.

Bengtsson, H. (2025). rw: CLI for webR with Sandboxing Features. R Consortium Funded Projects.

Beven, K. (2016). Facets of uncertainty: Epistemic uncertainty, non-stationarity, likelihood, hypothesis testing, and communication. Hydrological Sciences Journal, 61(9), 1652–1665.

Beven, K., & Binley, A. (1992). The future of distributed models: Model calibration and uncertainty prediction. Hydrological Processes, 6(3), 279–298.

Boyle, D. P., Gupta, H. V., & Sorooshian, S. (2000). Toward improved calibration of hydrologic models: Multiple and noncommensurable measures of information. Water Resources Research.

Cho, K., & Kim, Y. (2022). Enhancing streamflow simulations through forecasting the residual errors of WRF-Hydro using LSTM. Water Resources Research.

Clark, M. P., Vogel, R. M., Lamontagne, J. R., et al. (2021). The abuse of popular performance metrics in hydrologic modeling. Water Resources Research, 57(9).

Cosgrove, B. A., Clark, E. P., Flowers, T., Graziano, T. M., & Ogden, F. L. (2024, December). Advancing NOAA National Water Model Operations with the NextGen Framework. In AGU Fall Meeting Abstracts (Vol. 2024, pp. H21C-01).

Demir, I., Xiang, Z., Demiray, B., & Sit, M. (2022). WaterBench-Iowa: a large-scale benchmark dataset for data-driven streamflow forecasting. *Earth system science data*, *14*(12), 5605-5616.

Di Matteo, L., Cambi, C., Ortenzi, S., Manucci, A., Venturi, S., Fronzi, D., & Valigi, D. (2026). ERA5-Land Data for Understanding Spring Dynamics in Complex Hydro-Meteorological Settings and for Sustainable Water Management. Sustainability, 18(2), 970.

Downer, C. W., Ogden, F. L., Martin, W. D., & Harmon, R. S. (2002). Theory, development, and applicability of the surface water hydrologic model CASC2D. Hydrological processes, 16(2), 255-275.

Duan, Y., Akula, S., Kumar, S., Lee, W., & Khajehei, S. (2023). A hybrid physics–AI model to improve hydrological forecasts. Artificial Intelligence for the Earth Systems, 2(1), e220023.

Ebert-Uphoff, I., Thompson, D. R., Demir, I., Gel, Y. R., Karpatne, A., Guereque, M., ... & Smyth, P. (2017). A vision for the development of benchmarks to bridge geoscience and data science. In *17th international workshop on climate informatics*.

Erazo Ramirez, C., Sermet, Y., Molkenthin, F., & Demir, I. (2022). HydroLang: An open-source web-based programming framework for hydrological sciences. Environmental Modelling & Software, 157, 105525.

Erazo Ramirez, C., Sermet, Y., & Demir, I. (2023). HydroLang Markup Language: Community-driven web components for hydrological analyses. Journal of hydroinformatics, 25(4), 1171-1187.

Erazo Ramirez, C., Sermet, Y., & Demir, I. (2024). HydroCompute: An open-source web-based computational library for hydrology and environmental sciences. Environmental Modelling & Software, 175, 106005.

Ewing, G., Mantilla, R., Krajewski, W., & Demir, I. (2022). Interactive hydrological modelling and simulation on client-side web systems: an educational case study. *Journal of Hydroinformatics*, *24*(6), 1194-1206.

Ewing, G., Erazo Ramirez, C., Vaidya, A., & Demir, I. (2024). Client-side web-based model coupling using basic model interface for hydrology and water resources. *Journal of Hydroinformatics*, *26*(2), 494-502.

Feng, D., Lawson, K., & Shen, C. (2020). Mitigating prediction error of deep learning streamflow models in large data-sparse regions. Geophysical Research Letters, 47(14).

Frame, J. M., Nearing, G. S., Kratzert, F., Raney, A., Rahman, M., & Salas, F. (2020). Improving US National Water Model Streamflow with Long Short-Term Memory 2 Networks. J. Am. Water Resour. Assoc.

Gochis, D. J., Barlage, M., Cabell, R., et al. (2020). The WRF-Hydro modeling system technical description (Version 5.1.1). NCAR Technical Note, 107.

Gupta, H. V., Kling, H., Yilmaz, K. K., & Martinez, G. F. (2009). Decomposition of the mean squared error and NSE performance criteria: Implications for improving hydrological modelling. Journal of Hydrology, 377(1-2), 80–91.

Gupta, H. V., Perrin, C., Blöschl, G., et al. (2014). Large-sample hydrology: a need to balance depth with breadth. Hydrology and Earth System Sciences, 18(2), 463-477.

Hafen, K. C., Blasch, K. W., Gessler, P. E., Sando, R., & Rea, A. (2022). Precision of headwater stream permanence estimates from a monthly water balance model in the Pacific Northwest, USA. Water, 14(6), 895.

House, E., Meselhe, E., Muste, M., & Demir, I. (2025). Streamflow hysteresis analysis through a deep-dive budget of the St Venant equation momentum terms. Water resources research, 61(8), e2024WR038103.

Hughes, M., Jackson, D. L., Unruh, D., et al. (2024). Evaluation of retrospective national water model soil moisture and streamflow for drought-monitoring applications. Journal of Geophysical Research: Atmospheres, 129(1), e2023JD038522.

Islam, S. S., & Demir, I. (2026). A novel methodology for enhancing flood risk communication: The nines of safety. *Cambridge Prisms: Water*, *4*, e8.

Jaeger, K. L., Hafen, K. C., Dunham, J. B., Fritz, K. M., Kampf, S. K., Barnhart, T. B., ... & Dunn, S. B. (2021). Beyond streamflow: Call for a national data repository of streamflow presence for streams and rivers in the United States. Water, 13(12), 1627.

Johnson, J. M., Munasinghe, D., Eyelade, D., & Cohen, S. (2019). An integrated evaluation of the National Water Model (NWM)-Height above nearest drainage (HAND) flood mapping methodology. Natural Hazards and Earth System Sciences, 19(11), 2405–2420.

Jolliffe, I. T., & Stephenson, D. B. (2011). Epilogue: New directions in forecast verification. Forecast verification: A practitioner's guide in atmospheric science, 221-230.

Joseph, J. F., & Guillaume, J. H. (2013). Using a parallelized MCMC algorithm in R to identify appropriate likelihood functions for SWAT. Environmental modelling & software, 46, 292-298.

Kavetski, D., Kuczera, G., & Franks, S. W. (2006). Bayesian analysis of input uncertainty in hydrological modeling: 1. Theory. Water resources research, 42(3).

Kirchner, J. W. (2006). Getting the right answers for the right reasons: Linking measurements, analyses, and models to advance the science of hydrology. Water Resources Research, 42(3), W03S04.

Kizilkaya, D., Sajja, R., Sermet, Y., & Demir, I. (2025). Toward HydroLLM: a benchmark dataset for hydrology-specific knowledge assessment for large language models. *Environmental Data Science*, *4*, e31.

Kling, H., Fuchs, M., & Paulin, M. (2012). Runoff conditions in the upper Danube basin under an ensemble of climate change scenarios. Journal of Hydrology, 424, 264-277.

Knoben, W. J. M., Freer, J. E., & Woods, R. A. (2019). Technical note: Inherent benchmark or not? Comparing Nash–Sutcliffe and Kling–Gupta efficiency scores. Hydrology and Earth System Sciences, 23(10), 4323-4331.

Krajewski, W. F., Ghimire, G. R., Demir, I., & Mantilla, R. (2021). Real-time streamflow forecasting: AI vs. Hydrologic insights. *Journal of Hydrology X*, *13*, 100110.

Krause, P., Boyle, D. P., & Bäse, F. (2005). Comparison of different efficiency criteria for hydrological model assessment. Advances in Geosciences, 5, 89-97.

Kuczera, G., Kavetski, D., Renard, B., & Thyer, M. (2007). Bayesian total error analysis for hydrologic models: Markov Chain Monte Carlo methods to evaluate the posterior distribution. *Mod. and Simul. Soc. of Aust. and NZ, Christchurch, NZ*.

Lane, R. A., Coxon, G., Freer, J., Seibert, J., & Wagener, T. (2022). A large-sample investigation into uncertain climate change impacts on high flows across Great Britain. Hydrology and Earth System Sciences, 26(21), 5535-5554.

Legates, D. R., & McCabe, G. J. (1999). Evaluating the use of "goodness-of-fit" measures in hydrologic and hydroclimatic model validation. Water Resources Research, 35(1), 233-241.

Li, Z., Mount, J., & Demir, I. (2022). Accounting for uncertainty in real-time flood inundation mapping using HAND model: Iowa case study. *Natural Hazards*, *112*(1), 977-1004.

McCuen, R. H., Knight, Z., & Cutter, A. G. (2006). Evaluation of the Nash-Sutcliffe Efficiency Index. Journal of Hydrologic Engineering, 11(6), 597-602.

McKay, L., et al. (2012). NHDPlus Version 2: User Guide. US Environmental Protection Agency.

McMillan, H., Montanari, A., Cudennec, C., Savenije, H., Kreibich, H., Krueger, T., ... & Xia, J. (2016). Panta Rhei 2013–2015: global perspectives on hydrology, society and change. *Hydrological Sciences Journal*, *61*(7), 1174-1191.

Melsen, L. A., Puy, A., Torfs, P. J. J. F., & Saltelli, A. (2025). The rise of the Nash-Sutcliffe efficiency in hydrology. Hydrological Sciences Journal, 70(8), 1248-1259.

Mizukami, N., Rakovec, O., Newman, A. J., Clark, M. P., Wood, A. W., Gupta, H. V., & Kumar, R. (2019). On the choice of calibration metrics for "high-flow" estimation using hydrologic models. Hydrology and Earth System Sciences, 23(6), 2601-2614.

Moriasi, D. N., Arnold, J. G., Van Liew, M. W., Bingner, R. L., Harmel, R. D., & Veith, T. L. (2007). Model evaluation guidelines for systematic quantification of accuracy in watershed simulations. Transactions of the ASABE, 50(3), 885-900.

Moriasi, D. N., Gitau, M. W., Pai, N., & Daggupati, P. (2015). Hydrologic and water quality models: Performance measures and evaluation criteria. Transactions of the ASABE, 58(6), 1763-1785.

Muste, M., Lee, K., Kim, D., Bacotiu, C., Oliveros, M. R., Cheng, Z., & Quintero, F. (2020). Revisiting hysteresis of flow variables in monitoring unsteady streamflows. Journal of Hydraulic Research, 58(6), 867-887.

Muste, M., Kim, D., & Kim, K. (2025). Where and when should we be concerned about flow hysteresis?. In River Flow 2024 (pp. 804-808). CRC Press.

Nash, J. E., & Sutcliffe, J. V. (1970). River flow forecasting through conceptual models part I - A discussion of principles. Journal of Hydrology, 10(3), 282–290.

Newman, A. J., et al. (2015). Development of a large-sample watershed-scale routing and streamflow dataset for the contiguous USA. Hydrology and Earth System Sciences, 19.

Niu, G.-Y., et al. (2011). The community Noah land surface model with multiparameterization options (Noah-MP). Journal of Geophysical Research: Atmospheres, 116(D12).

Paredes, I. (2025). R in the Browser: Announcing our WebAssembly distribution. Jupyter Blog.

Price, A. N., Jones, C. N., Hammond, J. C., Zimmer, M. A., & Zipper, S. C. (2021). The drying regimes of non-perennial rivers and streams. *Geophysical Research Letters*, *48*(14), e2021GL093298.

Pizarro, A., Koutsoyiannis, D., & Montanari, A. (2025). Combining uncertainty quantification and entropy-inspired concepts into a single objective function for rainfall-runoff model calibration. Hydrology and Earth System Sciences, 29(19), 4913–4928.

Pursnani, V., Sermet, Y., & Demir, I. (2025). A conversational intelligent assistant for enhanced operational support in floodplain management with multimodal data. *International Journal of Disaster Risk Reduction*, *122*, 105422.

Putman, A. L., Longley, P. C., McDonnell, M. C., Reddy, J., Katoski, M., Miller, O. L., & Brooks, J. R. (2024). Isotopic evaluation of the National Water Model reveals missing agricultural irrigation contributions to streamflow across the western United States. *Hydrology and earth system sciences*, *28*(13), 2895-2918.

Rafieeinasab, A., Mazrooei, A., Enzminger, T., Srivastava, I., Dugger, A., Gochis, D., ... & Schneider, T. (2024). A WRF-Hydro-based retrospective simulation of water resources for US integrated water availability assessment. Hydrology and Earth System Sciences Discussions, 2024, 1-37.

Ritter, A., & Muñoz-Carpena, R. (2013). Performance evaluation of hydrological models: Statistical significance for reducing subjectivity in goodness-of-fit assessments. Journal of Hydrology, 480, 33-45.

Sadler, J. M., Appling, A. P., Read, J. S., Oliver, S. K., Jia, X., Zwart, J. A., & Kumar, V. (2022). Multi-task deep learning of daily streamflow and water temperature. *Water Resources Research*, *58*(4), e2021WR030138.

Santos, L., Thirel, G., & Perrin, C. (2018). Pitfalls in using log-transformed flows within the KGE criterion. Hydrology and Earth System Sciences, 22(8), 4567-4581.

Sit, M., Seo, B. C., & Demir, I. (2021). Iowarain: A statewide rain event dataset based on weather radars and quantitative precipitation estimation. *arXiv preprint arXiv:2107.03432*.

Sivelle, V., Cinkus, G., Mazzilli, N., Labat, D., Arfib, B., Massei, N., ... & Jourde, H. (2023). Improvement of the KarstMod modeling platform for a better assessment of karst groundwater resources. Hydrology and Earth system sciences discussions, 2023, 1-26.

Schaefli, B., & Gupta, H. V. (2007). Do Nash values have value? Hydrological Processes, 21(15), 2075-2080.

Schoups, G., & Vrugt, J. A. (2010). A formal likelihood function for parameter and predictive inference of hydrologic models with correlated, heteroscedastic, and non-Gaussian errors. Water Resources Research, 46(10), W10531.

Seo, B. C., Krajewski, W. F., & Quintero, F. (2018). Multi-Scale Hydrologic Evaluation of the National Water Model Streamflow Data Assimilation. Water Resources Research.

Shi, H., & Cai, X. (2025). Extrapolability improvement of machine learning-based evapotranspiration models via domain-adversarial neural networks. Environmental Modelling & Software, 187, 106383.

Shortridge, J. E., Guikema, S. D., & Zaitchik, B. F. (2016). Machine learning methods for empirical streamflow simulation. Journal of Hydrology, 538, 724-738.

Smith, T., & Marshall, L. (2008). Bayesian methods in hydrologic modeling: A review. Journal of Hydrology.

Stagg, G. (2023). webR 0.1.0 has been released. Tidyverse Blog.

Tang, G., Clark, M. P., Papalexiou, S. M., Ma, Z., & Newman, A. J. (2021). Have satellite precipitation products improved over last two decades? Remote Sensing of Environment, 240, 111697.

Thébault, C., Perrin, C., Andréassian, V., Thirel, G., Legrand, S., & Delaigue, O. (2024). Multi-model approach in a variable spatial framework for streamflow simulation. *Hydrology and Earth System Sciences*, *28*(7), 1539-1566.

Tolson, B. A., & Shoemaker, C. A. (2007). Dynamically dimensioned search algorithm for computationally efficient watershed model calibration. Water Resources Research, 43(1), W01413.

Vrugt, J. A., ter Braak, C. J. F., Clark, M. P., Hyman, J. M., & Robinson, B. A. (2008). Treatment of input uncertainty in hydrologic modeling: Doing hydrology backward with Markov chain Monte Carlo simulation. Water Resources Research, 44(12), W00B09.

Vrugt, J. A., ter Braak, C. J. F., Diks, C. G. H., Robinson, B. A., Hyman, J. M., & Higdon, D. (2009). Accelerating Markov chain Monte Carlo simulation by differential evolution with self-adaptive randomized subspace sampling. International Journal of Nonlinear Sciences and Numerical Simulation, 10(3), 273-290.

Weijs, S. V., Schoups, G., & van de Giesen, N. (2010). Why hydrological predictions should be evaluated using information theory. Hydrology and Earth System Sciences, 14(12), 2545–2558.

Yilmaz, K. K., Gupta, H. V., & Wagener, T. (2008). A process-based diagnostic approach to model evaluation: Application to the NWS distributed hydrologic model. Water Resources Research, 44(9), W09417.

Yucel, I., Onen, A., Yilmaz, K. K., & Gochis, D. J. (2015). Calibration and evaluation of a flood forecasting system: Utility of numerical weather prediction model, data assimilation and satellite-based rainfall. Journal of Hydrology, 523, 49-66.

Zhou, L., Liu, P., Gui, Z., Zhang, X., Liu, W., Cheng, L., & Xia, J. (2022). Diagnosing structural deficiencies of a hydrological model by time-varying parameters. Journal of Hydrology, 605, 127305.

**Supplementary Materials 1. Analytical Description**

**S1. Deterministic Analysis**

This section details the deterministic evaluation framework implemented within the Hydrological Model Evaluation System (HyMES), which audits streamflow predictions from physically-based, data-driven, and physics-informed machine learning models against observed streamflow data.

S1.1 Information-Theoretic Metric Decomposition

To identify specific sources of structural error beyond aggregate performance, the system decomposes model efficacy into physically interpretable statistical vectors. The primary diagnostic utilized for assessing distributional consistency is the extended Kling-Gupta Efficiency (KGE). This metric isolates three distinct components of model performance:

$$\mathrm{KGE} = 1 - \sqrt{(\mathrm{r} - 1)^2 + (\alpha - 1)^2 + (\beta - 1)^2}$$

Within this formulation, the Pearson correlation coefficient (r) measures the timing accuracy and the overall shape of the simulated hydrograph. The variability term ($\alpha$), calculated as the ratio of simulated to observed standard deviations ($\sigma_{\mathrm{sim}}/\sigma_{\mathrm{obs}}$), assesses the model's capacity to reproduce flow extremes and system variance. Finally, the bias term ($\beta$), defined as the ratio of simulated to observed means ($\mu_{\mathrm{sim}}/\mu_{\mathrm{obs}}$), quantifies the total volumetric water balance. A flawless model yields a KGE of 1, whereas values falling below −0.41 denote performance worse than a simple mean-flow benchmark.

The framework also evaluates the Nash-Sutcliffe Efficiency (NSE), which can be decomposed to reveal its relationship with KGE components:

$$\mathrm{NSE} = 2\alpha\mathrm{r} - \alpha^2 - \left(\frac{\beta - 1}{\mathrm{CV}_{\mathrm{obs}}}\right)^2$$

Here, $\mathrm{CV}_{\mathrm{obs}}$ represents the coefficient of variation for the observed data ($\sigma_{\mathrm{obs}}/\mu_{\mathrm{obs}}$). This specific decomposition demonstrates that NSE heavily penalizes bias in low-variability basins. To further evaluate the water budget, the platform calculates Volumetric Efficiency (VE), which quantifies the fraction of the observed streamflow volume that is correctly delivered by the simulation:

$$\mathrm{VE} = 1 - \sum \frac{\mathrm{Q}_{\mathrm{sim}} - \mathrm{Q}_{\mathrm{obs}}}{\mathrm{Q}_{\mathrm{obs}}}$$

Values approaching 1 signify accurate closure of the water budget. This is complemented by the Water Balance Error (WBE), expressed as a percentage, where positive values indicate a volumetric over-prediction and negative values indicate an under-prediction. The deterministic suite is completed by calculating the Root Mean Square Error (RMSE) and the coefficient of determination ($\mathrm{R}^2$) to provide a traditional error profile.

*Jensen-Shannon Divergence (JSD)*

The Jensen-Shannon Divergence (JSD) provides a symmetric measure of divergence between the marginal flow distributions of the observed (P) and simulated (Q) records. It utilizes a pointwise mixture distribution representing the mean probability mass, $M = \frac{P+Q}{2}$. The JSD is calculated as the average Kullback-Leibler (KL) divergence from both P and Q to this stabilizing mixture:

$$JSD(P|Q) = \frac{1}{2}KL(P|M) + \frac{1}{2}KL(Q|M)$$

By normalizing with a base-2 logarithm, the metric is strictly bounded to the interval [0, 1]. A JSD = 0 indicates identical marginal distributions, operating completely independent of temporal timing errors.

*Normalized Mutual Information (NMI)*

Normalized Mutual Information (NMI) quantifies the fraction of shared information and non-linear temporal dependence between the observed (X) and simulated (Y) time series. It calculates the shared information utilizing the marginal and joint Shannon Entropies (H) of the variables:

$$NMI = \frac{H(X) + H(Y) - H(X,Y)}{\sqrt{H(X) \cdot H(Y)}}$$

This derivation yields a dimensionless scalar bounded in [0,1]. An NMI = 1 indicates a perfect deterministic bijection, representing complete information overlap. This information-theoretic formulation detects complex, non-linear dependencies that the standard linear Pearson correlation coefficient systematically misses.

S1.2 Spatiotemporal Constraints and Boundary Conditions

Model predictions are subjected to physical audits across spatial networks and temporal states to ensure mechanistic validity. For networks of interconnected entities, a spatial continuity constraint is enforced:

$$Q_{out,\,upstream} + \sum \text{Local Gains} = Q_{in,\,downstream}$$

Violations of this constraint serve to identify either upstream mass-balance errors or unmodeled lateral inflows. Furthermore, hydrological memory is evaluated via the temporal gradient of storage ($\Delta S/\Delta t$). Sudden shifts in model-predicted storage that occur without corresponding input fluxes, such as precipitation or snowmelt, are systematically penalized to ensure temporal adjacency is maintained.

S1.3 Residual Analysis

Model residuals ($\varepsilon_t = Q_{obs,t} - Q_{sim,t}$) are treated as probability distributions to effectively isolate systematic biases. Residuals are initially binned into equal-width, density-normalized intervals so that the total area equals 1. A fitted Normal PDF is then overlaid onto the histogram to allow for a visual evaluation of normality

$$f(x) = \frac{1}{\widehat{\sigma\sqrt{2\pi}}} \exp\left(-\frac{(x-\hat{\mu})^2}{2\widehat{\sigma^2}}\right)$$

This assessment is supported by Quantile-Quantile (Q-Q) mapping, where theoretical Gaussian quantiles—estimated via the Beasley-Springer-Moro inverse CDF approximation—are plotted against the sample quantiles. Deviations from the 1:1 reference line highlight non-Gaussian error structures within the model. Finally, the framework computes explicit distributional statistics. Residual skewness is quantified utilizing the bias-corrected Fisher's moment, while excess kurtosis identifies heavy-tailed error distributions. A formal normality flag is registered for the residuals only when the absolute value of skewness is less than 0.5 and the absolute value of excess kurtosis is less than 1.

## S2. Uncertainty Quantification

This section outlines the probabilistic evaluation layer of the framework, which transforms point-estimate model outputs into physically-consistent probability distributions. The platform evaluates predictive uncertainty by executing specialized sampling engines operating entirely in the browser via WebR.

### S2.1 Physics-Informed Prior Constraints

Prior to executing the statistical algorithms, the system applies a two-step pipeline that translates physical hypotheses into statistical prior constraints on the uncertainty engine. This ensures domain knowledge informs the analysis without requiring re-execution of the underlying hydrological model. The Precipitation Gain scalar ($\mathrm{rainfallGain}$) simulates under- or over-received rainfall by pre-scaling model flows and setting the prior mean for the Markov Chain Monte Carlo (MCMC) bias parameter to $\beta_{\mathrm{prior}} = \mathrm{rainfallGain} - 1$. Hypotheses regarding initial watershed wetness determine the starting bias of the chains, calculated as $\beta_{\mathrm{init}} = (\mathrm{soilMoisture} - 0.5) \times 0.4$, where a dry condition initializes an over-predicting chain and a saturated condition initializes an under-predicting chain. Finally, the channel roughness coefficient $(\mathrm{n})$ directly modulates the upper bound for the heteroscedastic noise parameter $(\sigma_{\mathrm{r}})$ by enforcing a ceiling defined as $\mathrm{sr}_{\mathrm{max}} = \mathrm{clip}(0.1 + \mathrm{roughness} \times 3.5, 0.1, 0.8)$. Additionally, the roughness parameter applies a discrete temporal routing lag calculated as $\lfloor (\mathrm{n}/0.035 - 1) \times 2 \rfloor$ timesteps, clamped to $\pm 4$. At their neutral defaults (rainfallGain = 1.0, soilMoisture = 0.5, roughness = 0.035), these constraints revert to a standard, prior-free statistical analysis.

S2.2 Markov Chain Monte Carlo (MCMC) Framework

The primary sampling methodology utilizes an MCMC approach driven by a Metropolis-Hastings algorithm for Bayesian parameter estimation. The algorithm operates on two primary parameters: a relative noise multiplier ($\sigma_{\mathrm{r}} \in (0, 0.8)$) and a multiplicative bias correction ($\beta \in (-0.5, 0.5)$). The chains are initialized at $\sigma_{\mathrm{r}} = 0.25$ and $\beta = 0$, with new parameters proposed from an isotropic Gaussian distribution ($\sigma_{\mathrm{proposal}} = 0.02$). Proposals are accepted or rejected via the standard Metropolis criterion, discarding the first 20% of the chain as burn-in and applying a thinning interval of 5 to mitigate autocorrelation. Analysts can select between distinct observation likelihood functions. The standard Gaussian Likelihood assumes normally distributed errors proportional to the raw simulated flow:

$$\mathrm{Q}_{\mathrm{obs,t}} \sim \mathcal{N}\left(\mathrm{Q}_{\mathrm{NWM,t}} \cdot (1 + \beta),\ \sigma_{\mathrm{r}} \cdot \mathrm{Q}_{\mathrm{NWM,t}}\right)$$

Alternatively, a KGE-Based Likelihood evaluates the efficiency of the proposed simulation directly inside the MCMC step:

$$\mathrm{L}(\theta) \propto \exp\left(-\frac{(\mathrm{KGE}(\theta) - 1)^2}{2\sigma_{\mathrm{L}}^2}\right)$$

where $\sigma_{\mathrm{L}} = 0.2$. A log-transform option, which evaluates the likelihood on $\log(\mathrm{x} + 1)$ transformed arrays, is heavily recommended to stabilize variance across right-tailed streamflow distributions. Chain convergence is rigorously audited via the proposal acceptance rate (targeting

20–40%), the Effective Sample Size (ESS > 100), and the Geweke Z-score ($|Z| < 2$) to verify stationarity.

The primary sampling methodology utilizes an MCMC approach driven by a Metropolis-Hastings algorithm for Bayesian parameter estimation. The algorithm maps the joint posterior distribution of the parameter set $\theta = \{\sigma_r, \beta\}$, where $\sigma_r \in (0,0.8)$ represents a relative noise multiplier and $\beta \in (-0.5,\ 0.5)$ acts as a multiplicative bias correction. The chains are initialized at $\sigma_r = 0.25$ and $\beta = 0$, with new parameters proposed from an isotropic Gaussian distribution ($\sigma_{proposal} = 0.02$). Proposals are accepted or rejected based on their fit to the joint posterior via the standard Metropolis criterion:

$$\alpha_{accept} = \min\left(1,\ \frac{\pi(\theta^*|\mathbf{Z})}{\pi(\theta_{cur}|\mathbf{Z})}\right)$$

The first 20% of the chain is discarded as burn-in, and a thinning interval of 5 is applied to mitigate autocorrelation. The retained samples constitute the numerical approximation of the joint posterior, from which the predictive streamflow ensemble is subsequently drawn.

S2.3 Generalized Likelihood Uncertainty Estimation (GLUE) and ANOVA

As an alternative to Bayesian estimation, the platform implements GLUE based on the principle of equifinality. GLUE filters non-physical model realizations via Monte Carlo rejection sampling using uniform parameter priors ($\sigma_r \sim U(0.05,0.6)$ and $\beta \sim U(-0.4,0.4)$). A simulation is considered behavioral if its NSE satisfies a threshold constraint, defaulting to $\mathrm{NSE}(Q_{obs}, Q_{sim}) \geq 0.4$. If zero behavioral runs are found, this threshold is automatically relaxed by 0.2. The behavioral likelihoods are calculated as:

$$L(\theta|\mathbf{Z}) = \left[1 - \frac{\sigma_{err}^2}{\sigma_{obs}^2}\right]^N$$

These behavioral scores are normalized to sum to 1 and used as importance weights for bounding the posterior ensemble. For structural variance partitioning, the framework employs an Analysis of Variance (ANOVA) utilizing a Sobol-style methodology to estimate first-order sensitivity indices for $\sigma_r$ and $\beta$. To avoid full Sobol matrix computation, it leverages the Saltelli (2010) estimator via independent uniform sample matrices (A, B) and cross-sample matrices ($AB_1$, $AB_2$) to efficiently compute the indices:

$$S_{\sigma_r} = \frac{\mathrm{mean}\left[Y_B\left(Y_{AB_1} - Y_A\right)\right]}{V_{total}}, \quad S_{bias} = \frac{\mathrm{mean}\left[Y_A\left(Y_{AB_2} - Y_B\right)\right]}{V_{total}}$$

where Y represents the KGE of each simulation and $V_{total}$ is the total ensemble variance.

S2.4 Uncertainty Decomposition and Out-of-Sample Validation

The framework systematically decomposes predictive uncertainty into three explicit budgets. Aleatory uncertainty represents irreducible measurement noise, structural discrepancy is measured as the distance between the MCMC posterior mean and the deterministic baseline, and epistemic uncertainty is quantified via the information entropy of the uncertainty band (H):

$$H \approx \frac{1}{n}\sum_{t=1}^{n} \log\left(\Delta_{95\backslash\%,t} + \varepsilon\right)$$

where $\Delta_{95\backslash\%,t} = Q_{upper,t} - Q_{lower,t}$ defines the bandwidth at time step t. Out-of-sample performance is validated automatically on a held-out data period. The primary metric for this validation is the Continuous Ranked Probability Score (CRPS), which jointly rewards ensemble sharpness and calibration accuracy:

$$\mathrm{CRPS}(F, y) = \int_{-\infty}^{\infty} [F(z) - 1(z \geq y)]^2 dz$$

S2.5 Ensemble Diagnostics and Distribution Fitting

The physical reliability of the generated ensemble is evaluated utilizing a suite of structural indices. Calibration quality is quantified via the P-Factor, calculating the fraction of observations bracketed by the 95% predictive interval:

$$P = \frac{1}{n}\sum_{t=1}^{n} \mathbf{1}\left[Q_{lower,t} \leq Q_{obs,t} \leq Q_{upper,t}\right]$$

This is assessed alongside the R-Factor, measuring the normalized average bandwidth ($\overline{\Delta_{95\backslash\%}}/\sigma_{obs}$), with the goal of maximizing the P-Factor while minimizing the R-Factor.

Distributional dispersion is evaluated using a Talagrand rank histogram, computed by ranking observations against all N sorted ensemble members at each timestep:

$$\mathrm{rank}_t = \#\{m: Q_{sim}^{(m)}(t) < Q_{obs}(t)\} \in \{0,1, \dots, N\}$$

A perfectly reliable ensemble yields a flat histogram, while U-shaped or dome-shaped patterns highlight over-confidence and over-dispersion, respectively. This geometric shape is transformed into a continuous scalar via Rank Histogram Entropy ($H_{rank,norm}$), normalizing the Shannon entropy of the rank bins against a uniform distribution to yield a score bounded between 0 and 1. Diagnostic precision is further enhanced by calculating the metric arrays—including KGE and NSE—across three conditional flow regimes: High Flow (observations $> Q_{90}$), Mid Flow, and Low Flow (observations $< Q_{10}$). Temporal stability of the underlying residual bias is audited via the Pettitt change-point test:

$$K_T = \max_{1 \leq t \leq T}\left|U_{t,T}\right|, \quad U_{t,T} = \sum_{i=1}^{t}\sum_{j=t+1}^{T} \mathrm{sgn}\left(r_i - r_j\right)$$

A significant result ($p < 0.05$) points to a systematic temporal shift in model error, likely driven by physical or rating curve changes. Finally, the framework aggregates the per-run metric distributions across the ensemble utilizing Kernel Density Estimation (Sheather-Jones bandwidth for high fidelity) and fits parametric Gamma distributions via Maximum Likelihood Estimation to explicitly map performance variance.

**S3. Structural Diagnostics**

This approach extracts and compares diagnostic properties intrinsic to the time-series structure of both observed and simulated streamflow, providing information orthogonal to deterministic errors and predictive uncertainty bounds. By evaluating structural properties—such as flashiness, seasonality, and catchment memory—the framework identifies specific physical mechanisms that the model fails to reproduce.

S3.1 Temporal Stationarity, Trend, and Seasonality

Streamflow stationarity is formally assessed utilizing two complementary statistical tests to rigorously audit structural stability. The Augmented Dickey–Fuller (ADF) test evaluates the null hypothesis of a unit root, where rejection ($p < 0.05$) provides evidence for stationarity. Conversely, the Kwiatkowski–Phillips–Schmidt–Shin (KPSS) test evaluates the null hypothesis of stationarity itself. A time series is strictly classified as stationary only when the ADF test rejects non-stationarity ($p < 0.05$) and the KPSS test simultaneously fails to reject stationarity ($p > 0.05$).

Long-term temporal trajectories are quantified using the non-parametric Mann-Kendall (MK) test, which detects monotonic trends without assuming normality. The MK test statistic (S) and its variance are computed as:

$$S = \sum_{i=1}^{n-1} \sum_{j=i+1}^{n} \operatorname{sgn}(x_j - x_i)$$

$$\operatorname{Var}(S) = \frac{n(n-1)(2n+5)}{18}$$

These are used to derive the normalized Z score and Kendall's τ statistic ($\tau = S/\binom{n}{2}$), representing trend strength bounded between −1 and +1. The absolute magnitude of this trend is estimated via Sen's slope, representing the median change per time step in units of $m^3/s \cdot yr^{-1}$:

$$\widehat{Q} = \operatorname{median}\left(\frac{x_j - x_i}{j - i}\right), \quad \forall j > i$$

To maintain computational performance on extensive daily records, series are subsampled to a maximum of 500 points prior to MK computation.

Seasonal structures are isolated using Seasonal-Trend decomposition via Loess (STL), which partitions the series into trend ($T_t$), seasonal ($S_t$), and residual ($R_t$) components:

$$x_t = T_t + S_t + R_t$$

From this decomposition, the framework calculates continuous scalars for both seasonal strength ($F_s$) and trend strength ($F_t$):

$$F_s = \max\left(0,\ 1 - \frac{\operatorname{Var}(R_t)}{\operatorname{Var}(S_t + R_t)}\right), \quad F_t = \max\left(0,\ 1 - \frac{\operatorname{Var}(R_t)}{\operatorname{Var}(T_t + R_t)}\right)$$

Values approaching 1 indicate strong seasonal or trend structures relative to the residual noise. To prevent the fitting of spurious short cycles, an adaptive period detection logic is enforced: a period of 365 is applied if the record contains at least three full years of daily data (≥ 1095 points), while a period of 12 is utilized for records exhibiting at least three years of monthly proxy data. If sufficient data is unavailable, the STL decomposition is bypassed.

S3.2 Autocorrelation and Flow Duration Properties

Hydrological persistence is quantified through the sample Autocorrelation Function (ACF) and Partial Autocorrelation Function (PACF), computed for lags up to $\lfloor n/3 \rfloor$. Confidence bands are established at the asymptotic 95% interval of $\pm 1.96/\sqrt{n}$. The joint significance of the first h autocorrelations is tested utilizing the Ljung-Box test:

$$Q_{LB} = n(n+2)\sum_{k=1}^{h}\frac{\widehat{\rho_k^2}}{n-k} \sim \chi^2(h)$$

A p-value below 0.05 indicates statistically significant temporal persistence.

Flow distribution characteristics are extracted via the Flow Duration Curve (FDC), plotting flow magnitude against the exceedance probability $p_i = i/(n+1)$. The framework isolates discrete percentiles corresponding to specific physical regimes: $Q_{10}$ for high-flow stormflow dynamics, $Q_{50}$ for characteristic median flows, and $Q_{90}$ for low-flow baseflow contributions. The overall variability and flashiness of the system are represented by the FDC slope:

$$\text{FDC slope} = \log_{10}(Q_{10}) - \log_{10}(Q_{90})$$

S3.3 Signature Agreement and Composite Scoring

To systematically compare observed and simulated structural properties, the platform computes a dimensionless agreement score bounded between 0 and 1 for each evaluated pillar. The continuous metrics for FDC slope, median flow, and seasonal strength are evaluated via ratio-based penalty functions:

$$r_{slope} = S_{slope}^{sim}/S_{slope}^{obs} \Rightarrow \text{Score} = \max\left(0,\, 1 - \left|r_{slope} - 1\right|\right)$$
$$r_{Q50} = Q_{50}^{sim}/Q_{50}^{obs} \Rightarrow \text{Score} = \max\left(0,\, 1 - \left|r_{Q50} - 1\right|\right)$$
$$r_{Fs} = F_s^{sim}/F_s^{obs} \Rightarrow \text{Score} = \max(0,\, 1 - |r_{Fs} - 1|)$$

Categorical matches, such as trend direction and stationarity classification, yield a binary score of 1 for a match and 0 for a mismatch. The autocorrelation distance is calculated as the mean absolute error across the correlogram:

$$d_{ACF} = \frac{1}{L}\sum_{k}\left|\widehat{\rho_k^{obs}} - \widehat{\rho_k^{sim}}\right| \Rightarrow \text{Score} = \max(0,\, 1 - d_{ACF})$$

These individual sub-scores ($s_k$) are averaged and rescaled to generate a final Composite Signature Score ranging from 0 to 100:

$$\text{Signature Score} = 100 \times \frac{1}{K}\sum_{k=1}^{K} s_k$$

A score of 100 indicates perfect reproduction of all measurable structural properties. Scores ≥ 70 are classified as good, 40–70 as marginal, and below 40 as representing poor signature reproduction. While conceptually part of the distribution-level assessment (see S1.1), the Jensen-Shannon Divergence and Normalized Mutual Information metrics are incorporated into this analytical view to provide a holistic distribution fingerprint.

S3.4 Hysteresis and Catchment Memory

The physical partitioning of runoff into fast surface pathways and delayed subsurface pathways manifests as a temporal hysteresis effect, which the framework quantifies using a lagged Q–Q Hysteresis Index (HI). This index maps the streamflow $Q(t-k)$ against $Q(t)$ for a specified delay k, evaluating the closed loop formed by the rising and falling limbs of a hydrograph. The HI is derived from the signed shoelace-formula area of this polygon, normalized by the squared peak flow:

$$HI = \frac{\mathrm{SignedArea}(Q_{t-k}, Q_t)}{(Q_{max})^2}$$

A clockwise loop (HI > 0) indicates rapid surface-runoff pathways, where flow on the rising limb is higher than on the receding limb for an equivalent storage state. A counter-clockwise loop (HI < 0) signifies delayed peak flow typical of groundwater baseflow processes, while a symmetric loop ($|HI| \approx 0$) indicates equal kinematic spread without significant hysteresis.

To preserve the topological validity of the hydrograph, the HI computation utilizes a per-event extraction architecture. Peak detection is executed on a downsampled time series for performance; however, these indices are mapped back to the full-resolution arrays to extract independent temporal windows around each event. The HI is strictly computed on these full-resolution windows, either presented for individual events or aggregated as a mean with standard deviation. The model's structural reproduction of catchment memory is audited via the reproduction error ($\Delta HI = HI_{obs} - HI_{sim}$). Minor divergence ($|\Delta HI| \approx 0.01 - 0.03$) indicates lag parameterization errors, whereas severe mismatch ($|\Delta HI| > 0.03$) suggests the model is entirely missing a dominant physical runoff generation pathway.

**Supplementary Materials 2. Software Architecture and Development**

## 1. AI-Assisted Diagnostic Synthesis

To interpret the complex interplay across deterministic errors, probabilistic uncertainty bounds, and structural signatures, the platform integrates an AI Insight layer acting as a contextual synthesizer. This subsystem connects to Large Language Model backends (such as OpenAI, Gemini, or Anthropic) via user-configured API keys to generate window-specific, data-grounded interpretations.

The system programmatically constructs strictly formatted prompt payloads based on the analytical context. For the uncertainty window, the context explicitly differentiates raw baseline NWM performance from posterior calibrated ensemble KGE alongside MCMC convergence diagnostics. For the temporal window, it passes the explicit sub-score breakdown and monotonic trend markers, while the hysteresis window payload details loop geometries and limb asymmetries. To ensure scientific rigor, the AI is constrained by strict personas (e.g., "hydrometeorological data analyst"), explicitly forbidden from hallucinating uncomputed metrics, required to cite specific numbers to justify evaluations, and mandated to provide a singular actionable recalibration step. If external APIs are unavailable, the system successfully defaults to a deterministic, rule-based interpretation framework utilizing the same structured diagnostic data.

When no API key is configured, the deterministic fallback applies rule-based interpretations using the same data context. Rules cover:

- KGE / NSE severity thresholds (good ≥ 0.75, moderate ≥ 0.5, poor < 0.5)
- Regime asymmetry (high-flow vs. low-flow KGE difference > 0.2)
- FDC outlier detection (Q90 ratio < 0.6 = severe baseflow under-estimation)
- Pettitt change-point significance
- MCMC acceptance rate warning (< 10%)
- Stationarity and seasonal mismatch flags
- Hysteretic mismatch conditions (interpreting ΔHI scaling and physical meaning)

Table 1. Model Providers

| **Provider** | **Model** | **Key storage key** |
|---|---|---|
| OpenAI | gpt-4o | hymes_openai_key |
| Gemini | gemini-1.5-pro | hymes_gemini_key |
| Anthropic | claude-3-5-sonnet | hymes_anthropic_key |

Table 2. Metrics used from the uncertainty diagnostics.

| Category | Fields |
| --- | --- |
| Core deterministic (NWM baseline) | KGE, NSE, VE, RMSE, $R^2$, r, α, β, CV, WBE — these reflect the uncalibrated NWM directly vs. obs |
| Posterior ensemble distribution | Ensemble median KGE, P5 KGE, P95 KGE, ensemble median NSE — the primary UQ performance result |
| UQ indices | P-Factor, R-Factor |
| Information Theory | JSD, NMI, H_rank (rank entropy), H_band (band entropy) |
| Conditional regime | KGE + NSE for high / mid / low flow regimes (n per regime) |
| Validation | Val-KGE, Val-NSE, CRPS, n_cal, n_val |
| MCMC convergence | Acceptance rate, ESS(b), ESS(σ), Geweke Z(b), Geweke Z(σ), behavioral count |
| Pettitt change-point | Significant flag, date, bias before/after, p-value |
| FDC ratios | Q10, Q50, Q90 sim/obs ratios |
| Context | Station ID, NWM version, UQ method |

Table 3. Metrics used from the structural diagnostics.

| Category | Fields |
| --- | --- |
| Descriptive stats | obs/sim mean, obs CV, skewness |
| Stationarity | Stationary flag + AR(1) coef + variance ratio for both obs and sim |
| Trend | Direction, significance, Sen's slope (m3/s per step) for both |
| Seasonality | STL seasonal strength Fs, trend strength Ft, seasonal ratio; period used (12 or 365) |
| Autocorrelation | Ljung-Box p, autocorrelation flag for both |
| FDC | FDC slope ratio, FDC score, Q50 ratio |
| Distribution Fingerprint | JSD (marginal divergence), NMI (information overlap) |
| Signature sub-scores | FDC score, Q50, season score, ACF score, trend-match |

Table 4. Metrics used from the hysteresis analysis

| Category | Fields |
|---|---|
| Loop indices | Observed HI, simulated HI, ΔHI (obs−sim) reproduction error |
| Aggregation mode | Per-event (single event selected) or mean ± std across all detected events |
| Year filter | Calendar year of analysis, when year-level filter is active |
| Geometric dominance | Dominant loop direction (clockwise vs counter-clockwise vs symmetric) |
| Limb asymmetry | Rising limb fraction, falling limb fraction (from full-period limb classification) |
| Event framing | Number of detected flood peaks, analyzed event window label (year / all / specific event + date) |

Table 5. AI Expert personas used for structured diagnostic interpretation.

| AI Persona | Evaluation Focus | Diagnostics Consumed | Interpretation Role | Typical Output to User |
|---|---|---|---|---|
| Deterministic Performance Evaluator | Predictive accuracy and systematic error | NSE, KGE (and components r, α, β), RMSE, bias, water-balance error | Determines whether apparent skill reflects timing accuracy, variance reproduction, or volumetric bias; | Identifies dominant deterministic deficiency (e.g., bias-driven agreement, damped variability) |
| Uncertainty & Robustness Evaluator | Sensitivity and reliability under uncertainty | Ensemble metric distributions, P-factor, R-factor, CRPS, rank-histogram entropy | Assesses calibration, sharpness, and robustness of deterministic performance; distinguishes stable from fragile skill | Flags over-confident, over-dispersed, or poorly calibrated ensembles |
| Structural Behavior Evaluator | Hydrological realism and system behavior | Flow Duration Curve metrics, seasonal strength, persistence and autocorrelation scores, information-theoretic signatures | Evaluates whether simulations that appear accurate reproduce physically meaningful flow structure | Identifies regime-specific inconsistency or structural mismatch |
| Hysteresis (Catchment Memory) Evaluator | Dynamic response and lagged flow behavior | Hysteresis Index (HI), ΔHI, loop orientation and geometry | Tests reproduction of observed catchment memory and runoff pathway dominance | Confirms or rejects agreement in dynamic response despite aggregate performance |
| Synthesis (Integrated Reasoner) | Cross-layer consistency | Outputs from all personas | Integrates evidence across deterministic, probabilistic, structural, and hysteretic layers | Produces a concise, number-driven diagnostic summary and one recommended next analytical step |

Table 6. Results from the AI evaluator for the anchor station.

| **Evaluation Level** | **NWM 2.1** | | | **NWM 3.0** | | |
|---|---|---|---|---|---|---|
| | Structural Evaluator | Hysteresis Evaluator | UQ Evaluator | Structural Evaluator | Hysteresis Evaluator | UQ Evaluator |
| Primary Metric | The FDC slope ratio of 0.84 combined with the ACF mean distance of 0.196 indicates that the model is too damped, underestimating variability in the observed variable series. | The ΔHI of 0.009 indicates a minor loop mismatch, suggesting that the model's lag or routing parameterization may not adequately capture the dynamics of surface runoff. | The high bias ratio of 1.659 combined with a negative KGE of -0.038 indicates significant over-estimation of the observed variable across the simulation. | The FDC slope ratio of 0.86 combined with the ACF mean distance of 0.196 points to a model that is too damped, underestimating variability in the observed variable. | The HI_obs of 0.009 combined with HI_sim of -0.001 indicates a significant divergence in the model's ability to replicate surface runoff dynamics, as evidenced by the ΔHI of 0.010. | The posterior ensemble KGE of -0.046 combined with a high water balance error of 51.2% indicates significant discrepancies between the model simulation and observed variable, particularly in capturing the observed variability. |

| Evaluation Level | NWM 2.1 | | | NWM 3.0 | | |
|---|---|---|---|---|---|---|
| Cross Checking | The significant autocorrelation in both observed and simulated series suggests that the model captures some temporal dependencies, but the mismatch in the FDC slope ratio highlights a structural inconsistency. | The clockwise loop character with HI_obs at 0.009 confirms that the surface runoff pathway is dominant, aligning with the observed behavior during flood events. | The JSD of 0.536 confirms a distribution mismatch, highlighting a lack of alignment between observed and simulated values. | The significant autocorrelation in both observed and simulated series suggests consistency in temporal dependencies, despite the damped response indicated by the FDC metrics. | The clockwise loop character confirms that the observed data is indeed dominated by surface runoff, which aligns with the HI values. | The JSD of 0.477 confirms a distribution mismatch, highlighting that the model's output diverges considerably from the observed data. |